Tokyo University of Agriculture and Technology

DOCTORAL THESIS

Real-time EEG Oscillatory Phase Prediction and Phase-Informed Visual Stimulation Using a Least Mean Square-based AR Model

---

Author:

Aqsa Shakeel

Supervisor:

Dr. Toshihisa Tanaka

Dr. Keiichi Kitajo

A thesis submitted in fulfillment of the requirements
for the degree of Doctor of Philosophy

in the

Department of Electronics and Information Engineering

January 27, 2021

Authorship Declaration

I, Aqsa Shakeel, declare that this thesis titled "**Real-time EEG Oscillatory Phase Prediction and Phase-Informed Visual Stimulation Using a Least Mean Square-based AR Model**" is entirely my original work. I confirm that:

This work was done entirely while in submission for a Ph.D. degree at Tokyo University of Agriculture and Technology (TUAT).

It has been clearly stated where any part of this thesis has been submitted previously at TUAT or any other institute.

It is always clearly attributed and referred to as the published work of other authors.

I have shown clearly what my contributions were and what was done by others.

Signed: Aqsa Shakeel

Date: 27-01-2021

“After you make a fool of yourself a few hundred times, you learn what works.”

Gwen Stefani

ABSTRACT

Background: The spontaneous oscillatory activity of neuronal networks is considered to be the most prominent feature of the rapidly changing brain state measured by EEG. This brain state can be computed using the instantaneous phase and amplitude; however, assessing the brain state in a real-time closed-loop setup is a technically intricate problem because, in order to define the current state, the future signal prediction is necessary, for example, instantaneous phase and amplitude. Alpha oscillations are thought to represent inhibitory or idling of cortical activities that are not related to a particular task. Nonetheless, recent studies on the alpha oscillation phase scrutinize that they have a direct and dynamic role in working memory and attention. To study the role of these oscillations, accurate phase estimation is required. A conventional Yule-Walker (YW)-based autoregressive (AR) model has been employed to achieve this in real-time. However, an adaptive approach for both the time-series forward prediction and the brain state-dependent real-time implementation of a closed-loop system so far has not been investigated.

Objectives: The primary objectives were; to evaluate the performance of an adaptive least mean square (LMS) based AR model and a conventional YW based AR model for time-series forward prediction in an offline study; to check the implementability of a time-series forward prediction employing an adaptive LMS-based AR model in a real-time closed-loop system.

Method: For time-series forward prediction, EEG data from twenty-one healthy participants were recorded for three minutes in the eyes-closed resting state. For the real-time closed-loop system, state-dependent EEG-triggered visual stimulation synchronizes with the peaks and troughs of EEG alpha oscillations in a visual task and an eyes-open resting task from nine participants. Participants were asked to focus passively on the fixation cross presented at the screen's midpoint for an eyes-open resting task. Whereas for the visual task, participants were presented with a 7x7 checkerboard stimulus with a fixation cross at the center. They were trained to click the left mouse button promptly when the fixation cross turns red.

Results: Two diverse prediction lengths of 128 ms and 256 ms were tested for both methods in an offline study. For real-time closed-loop implementation, both methods tested the prediction length of 85 samples (170 ms). The results of the offline study show that for the prediction of shorter length (128 ms), the Yule-Walker-based AR model surpasses the LMS-

based AR model, whereas for predicting the longer duration of 256 ms, the LMS-based AR model outperforms the conventional Yule-Walker based AR model.

In the real-time closed-loop system, resting peak condition, both methods showed statistically significant results in 100% of participants (five out of five participants). While for the trough condition, LMS showed statistically significant results in 100%, and YW showed 80% of participants. In the visual task, all participants in both methods and both conditions showed significant results.

Significance: The findings indicated that the LMS-based AR model with a low computational load was effectively applied in a real-time closed-loop system aiming at particular alpha oscillation phases and could be utilized as an adaptive substitute to the machine-learning and conventional methods.

Keywords:

Electroencephalography (EEG); Alpha oscillation; Autoregressive (AR) model; Yule-Walker (YW)-based AR model; Instantaneous phase; Least mean square (LMS); Time-series prediction; Brain state-dependent stimulation.

ACKNOWLEDGEMENTS

Uttermost thanks to Almighty Allah for countless blessings of my life. I am highly grateful to my parents for their sacrifices to corroborate that I was educated adequately and write this thesis. I am thankful to my siblings for their prayers, guidance, care, and remarkable support from the beginning of my life.

I am wholeheartedly thankful to my supervisors, Dr. Toshihisa Tanaka and Dr. Keiichi Kitajo, for their enormous support, sincere guidance, patience, and encouragement. Their supervision was a one of a kind and extraordinary experience for me. I am highly gratified to Dr. Kitajo, who nudged me often in the right direction.

I am incredibly thankful to Dr. Takayuki Onojima for always being accessible and providing valuable suggestions. Without his beneficial feedback, I wouldn't have learned as much as I had.

My appreciation goes to my extraordinary husband, Usman Abid Khan, for his patience, love, and support. I am obliged to Kaori Maeda to support experiments and all the volunteers who participated in my study.

AQSA SHAKEEL

To

My Parents

“Ammi, Abbu Ji”

& My Baby

“Muhammad Musab Usman Khan”

Contents

List of Tables

List of Figures

List of Abbreviations

LFP	Local field potential
EEG	Electroencephalography
AR model	Autoregressive model
YW	Yule-Walker
LMS	Least mean square
BCI	Brain-computer interface
ERD	Event-related desynchronization
NIBS	Non-invasive brain stimulation
TMS	Transcranial magnetic stimulation
MSE	Mean squared error
IAF	Individual alpha frequency
FIR	Finite impulse response
AIC	Akaike information criterion
PLV	Phase locking value
PLF	Phase locking factor
PLVrz	Rayleigh's Z value
SD	Standard deviation
AC	Alternating current
DC	Direct current
TTL	Transistor-transistor logic
LCD	Liquid crystal display
PTR	Phase triggered response
ERP	Event-related potential
CNN	Convolutional neural network
PCA	Principal component analysis
ms	Milliseconds
s	Seconds
SCNN	Simplified convolutional neural network
PD	Parkinson's disease
SNR	Signal-to-noise ratio

PART I

INTRODUCTION

1 Introduction

Neural oscillations changing rapidly are considered as vital characteristics of a nervous system. These neural oscillations in a single neuron might be viewed as periodic changes in one of two spiking behavior at the cellular level or potential at the subthreshold membrane. The synchronous activity produced by neurons extensive networks leads to periodic oscillations in the local field potential (LFP), reflecting neurons' excitability. The synchronous excitation [1] of neurons across a massive network facilitates brain communication. At specific frequencies, oscillations originate through particular tasks, which governs their power or amplitude [2].

1.1 Alpha Oscillations

Alpha oscillations usually have been a persistent feature of neural activity; but, their role has been confirmed by current studies in attention [3] and active inhibition [4, 5]. In older subjects, alpha frequencies are slow-going and apt towards frontal distribution [6]. The highest amplitude of alpha at the scalp is perceived over the brain's parietal and occipital cortices [7]. Furthermore, they are also visible as mu rhythms above motor areas [8]. Moreover, such studies mention that alpha oscillations with distinct functions in cognitive, perceptual, and motor processes play a particular part in brain information processing. Still, their role is yet to be discovered. Estimating an instantaneous phase and amplitude accurately and precisely are necessary to comprehend their role in motor, perceptual, and cognitive aspects. Because of time-frequency domain analysis, instantaneous phase relationships are categorized as post-hoc in majority of the investigations. The oscillatory phase's emphasis only does not infer that the amplitude of occurring oscillations does not affect. In reality, if the signal has sufficient amplitude, then the oscillatory phase of a signal can be computed reliably, both in the biophysical and mathematical sense. The instantaneous amplitude of electroencephalography (EEG) oscillations in several frequency bands endure substantial relations to attention and sensory perception [3, 7, 9, 10], while the instantaneous frequency has also been studied [11-13].

Until recent studies, the phase of ongoing oscillations has been mainly neglected, demonstrating the instantaneous phase's consequences on perceptual performance [14, 15]. Accurate and precise estimation of the instantaneous phase in real-time is vital to reveal their functional role. Assuming sufficiently narrow bandwidth, analog circuits were constructed in 1988 by Pavlides [16] and 1997, Holscher [17] that elicited stimulation at the zero crossings, peak, and trough of the LFP of the hippocampus. In theta oscillation for peak detection, Hyman

[18] applied a dual-window discrimination technique. Manual calibration was required in a specific setting in the study mentioned above; consequently, the real-time set-up would not be possible. Previous benchmark studies [19-21] optimized parameters using a genetic algorithm before algorithm deployment. The optimization procedure required particular computational measures and could not, therefore, be applied in real-time. To avoid implementing an offline optimization procedure before online implementation, the algorithm proposed in the studies mentioned earlier may be enhanced by choosing an online approach [19]. One alternative for instantaneous phase estimation uses the robust method, i.e., wavelet ridge extraction [22]. However, this method is suitable for variable multiple oscillations presented concurrently, perhaps computationally expensive for implementing in real-time. Edge effects might also constrain a real-time implementation because of the data's availability only in the reverse direction. Another substitute for EEG phase estimation in real-time applications is machine learning applied by McIntosh and Sajda [23]. Their proposed technique can be used in offline study as a substitute for non-causal filtering for the assessment of the phase. Still, the major shortcomings comprise the possibility of unbiased phase estimation and preliminary data for training. Hence, an adaptive technique is required for phase estimation in real-time.

Herein, we propose for time-series forward prediction, an adaptive technique least mean square (LMS)-based autoregressive (AR) model that was established based on the conventional Yule-Walker (YW)-based AR model [19, 20] with a continuation of an adaptive LMS-based AR model. To calculate AR coefficients, numerous algorithms might be used to construct the AR model, every one of them achieving diverse objectives. These approaches minimalize the error in prediction, either forward and backward direction or only forward prediction error. Our primary focus centers on the prediction error in the forward direction only and determines that the proposed adaptive method reduces the forward prediction error as it can adjust its coefficients dynamically and achieves better prediction results for longer lengths. As adaptive techniques can trace the coefficients dynamically and permit further precise predictions, the LMS-based AR model was chosen. Utilizing visual alpha oscillations, our primary interest was an estimation of the current instantaneous phase so that one can determine to provide the oscillatory phase-dependent stimulation or not. A novel brain-computer interface (BCI) technique can be perceived by implementing a closed-loop brain-state-dependent stimulation system.

1.2 Closed-Loop System

Closed-loop neuroscience is gaining more consideration with ongoing technical and innovative advances, thus enabling intricate feedback loops to be executed with a millisecond

resolution. Much has been studied about brain mechanics about “open-loop” stimulation via pre-determined stimuli, such as determining input-output properties and how they are possibly modified. In the non-invasive brain stimulation (NIBS) domain, this open-loop technique has been quite useful, facilitating significant developments in pharmacological understanding and knowing the functional basis of cortical dynamics [24, 25]. An experiment might be viewed as a “closed-loop” once the brain’s output becomes the brain’s future input. By constructing a causal link between the stimulus generator and the measured result, one can possibly “close the loop” [26] in the laboratory. In actuality, this can be accomplished when a presented stimulus depends on the instantaneous brain state estimated simultaneously. On that account, the brain's neuronal output affects the brain's input, thus closing the loop [26].

Combining EEG and transcranial magnetic stimulation (TMS) [27] presents closed-loop NIBS capability, accentuated by the recent accessibility of cost-effectiveness real-time processors. Although TMS has been at hand for numerous decades, it remains the most effective means to excite a particular cortical neuron network non-invasively. It can perform this at a resolution of millimeters for spatial and resolution of microseconds for temporal domain [25, 28]. Theoretically, the EEG signal can represent the brain state instantaneously at a lower-dimension. Usage of TMS can be perceived as a vector leading to a new trajectory by modifying a spontaneous brain state[29]. Remarkably, the new state attained by the TMS is reliant on the state of the brain at the respective time of stimulation. Therefore, it leads to the inspiration for developing paradigms of the closed-loop brain state-dependent stimulation.

In the current study, the emphasis was on the most prominent feature of the brain's state, i.e., neuronal networks' spontaneous oscillatory activity [30]. On a spatial scale, the state of interest could be observed locally, e.g., a particular brain area’s activity [31] or a large scale, for example, a brain network’s ensemble activity [32]. On the other hand, temporally, brain states can be determined in a specific frequency band by spectral power variations (such as event-related desynchronization [ERD]), also observing the phase-state of an oscillating cycle. This prior method has been efficiently utilized in brain-machine interfaces for both alpha rhythms (8–12 Hz) [33] and beta rhythms (16–22 Hz) [34], allowing stroke patients to execute robot-assisted motor tasks. Practically, “closing the loop” is quite intricate for both the spectral power and the instantaneous phase because real-time signal processing requires milliseconds resolution; nonetheless, such a time resolution has become attainable over the past decade [34-36]. Implementing a closed-loop system involves numerous technically demanding stages: signal processing, measuring output of the brain, and tuning/adjustment of the stimulus. With latest advancements in information technology, this combination of techniques has become

practicable thus permitting intricate calculations to be executed in real-time using cost effective equipment.

Our offline analysis study [37] compared conventional YW-based and adaptive LMS-based AR models and suggested the aforementioned adaptive methodology for time-series forward prediction. The offline study's main aims are an accurate and precise estimation of alpha oscillation's instantaneous phase using the adaptive approach and comparing adaptive and conventional techniques. The second part of the current study is an extension of our offline work, i.e., real-time implementations of conventional YW-based AR and adaptive LMS-based AR models. We designed an EEG-triggered visual stimulus closed-loop setup for the real-time implementation that synchronized the visual stimulus with ongoing alpha oscillation's particular phase from the occipital cortex. The prior benchmark study [19] implemented a YW-based AR model for estimating the instantaneous phase of intracranial EEG theta oscillations in real-time on two patients only. In comparison, a recent study [20] utilized a similar technique combined with TMS for mu rhythm phase estimation. The vital purpose was to confirm the implentability of an adaptive LMS-based AR model in real-time, along with a conventional one or not. Because of some technicalities in the direct current (DC) mode of EEG amplifiers, data recorded in the alternating current (AC) mode were analyzed only for a real-time closed-loop system, which led to a small number of participants. Therefore, the real-time closed-loop system did not confirm the adaptive method's advantage over the conventional one.

1.3 Autoregressive (AR) Model

AR modeling has been efficiently practiced in numerous applications of EEG analysis, like segmentation, forecasting [38, 39], and speech analysis [40]. Estimating the power spectrum of short duration EEG data, AR modeling displays excellent results because of its low exposure to false results [39]. Several algorithms can be utilized to calculate the coefficients of an AR model, comprising the Yule-Walker and Burg lattice algorithms.

An AR model is a random process of order *K* defined as follows[19]:

$$x(t+1) = \sum_{k=0}^{K-1} \alpha_k \, x(t-k) + \varepsilon_t, \qquad (1)$$

where $\alpha_0, \ldots, \alpha_{K-1}$ are coefficients of the AR model; *K* represents the model order; and ε_t is white noise.

Several algorithms can be used to calculate coefficients and construct an AR model, like the Yule-Walker technique, to minimalize the prediction error in the forward direction. The Burg lattice method uses the mean of squared-prediction errors in both backward and forward directions to solve the lattice filter equations. For comparison purposes with prior studies [19, 20], we utilized the Yule-Walker method. For this purpose, the order of the AR model was chosen by Akaike information criterion (AIC) [41].

1.4 Least Mean Square (LMS)

The AR model's primary purpose is to obtain the optimum coefficients minimalizing the mean squared error (MSE) recursively [42] for a random signal. In 1960, Hoff and Widrow developed the LMS algorithm [43]. It applies an iterative method of stochastic gradient descent to resolve the least square issue. The particular technique is acquired by substituting the desired Hessian matrices and gradient vectors with further appropriate estimations from the steepest-descent implementation. The adaptive LMS algorithm is established by the following equations [44]:

$$\boldsymbol{X}(t) = [x(t), x(t-1), x(t-2), \ldots \ldots x(t-K+1)]^T \quad (2)$$

$$\boldsymbol{A}(t) = [a_0(t), a_1(t), \ldots \ldots . a_{K-1}(t)]^T, \quad (3)$$

$$y(t) = \boldsymbol{A}^T(t)\boldsymbol{X}(t), \quad (4)$$

$$e(t) = x(t+1) - y(t), \quad (5)$$

$$\boldsymbol{A}(t+1) = \boldsymbol{A}(t) + 2\mu\, e(t)\boldsymbol{X}(t), \quad (6)$$

where $x(t)$ represents an input signal at sample t, $y(t)$ depicts the output, $e(t)$ is representing an error, the filter weight is indicated by $\boldsymbol{A}(t)$, μ denotes the step size, and K shows the order of the filter. The bold variables represent vectors.

In the offline study for forward prediction of time-series, conventional and adaptive methods were applied and compared. The conventional YW method calculates AR coefficients just one time, while the adaptive LMS method computes them instantly. The LMS algorithm without any prior information begins from an initial condition and, depending on the input data updating the filter weights. The filter size is similar to the YW-based AR model order. For ease, in the continuing text, we will use YW to denote the YW-based AR model and LMS to indicate the LMS-based AR model.

1.5 Instantaneous Frequency and Phase

The analytic signal is constructed to estimate the instantaneous phase due to combining original data with the original data's Hilbert transform [45]. So, the complex signal $z_x(t)$ can be created as:

$$z_x(t) = x(t) + iH\{x(t)\} \tag{7}$$

where x (t) represents the real signal and $H\{x(t)\}$ depicts the Hilbert transform of the real signal, which is defined as follows:

$$\mathrm{H}\{\mathrm{x}(t)\} = \frac{1}{\pi}\ \mathrm{P.V.} \int_{-\infty}^{\infty} \frac{\mathrm{x}(\tau)}{t-\tau}\ \mathrm{d}\tau, \tag{8}$$

where $\mathrm{P.V.}$ specifies Cauchy's principal value. The complex signal can now be utilized to find the instantaneous phase as follows:

$$\theta(t) = \arg z_x(t)\ . \tag{9}$$

PART II

OFFLINE STUDY

2 Materials and Methods

2.1 Outline of Algorithm

The algorithm's vital objective is to estimate the alpha oscillations' instantaneous phase and frequency by applying the YW and LMS-based AR model. The sequential steps for preprocessing in the algorithm are:

2.1.1 Preprocessing (YW and LMS):

1. Raw data were re-referenced, followed by downsampling to 500 Hz.
2. Frequency band optimization (8–13 Hz) centered on the highest frequency of every participant. The highest EEG power lying in the alpha range was related to the individual alpha frequency (IAF). The band-pass filter's passband was selected after obtaining the IAF. IAF-1 was the low cutoff frequency in the band-pass filter, and IAF+1 was the high cutoff frequency.
3. A two-pass finite impulse response (FIR) band-pass filter with an order of 128 and the passband selected in the 2nd step was implemented [46].
4. Data was divided into 500 milliseconds (ms) epochs.

2.1.2 YW-based AR model (reproducing Zrenner's approach) [20]:

1. Optimum AR model order was computed through AIC.m
2. Coefficients of the AR model were computed utilizing the Yule-Walker equations.
3. For predicting a length of 128 ms, the instantaneous phase was estimated at the edge of the sliding window in the AR equation [19, 20] Figure 1.

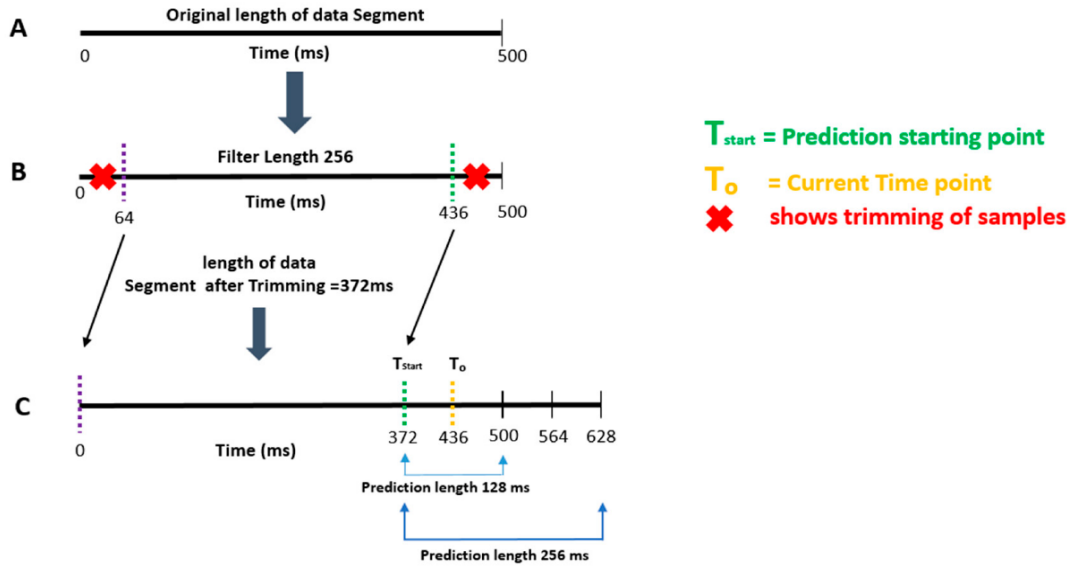

Figure 1 Time-series forward prediction based on the Autoregressive (AR) model. (**A**) The original data segment's length is 500 ms; (**B**) A 64ms data was cropped from both ends; (**C**) The residual data of 372 ms was utilized to compute AR coefficients for the prediction of 128 and 256 ms data.

2.1.3 LMS-based AR model:

1. The adaptation size or the learning rate was chosen for LMS.
2. Chose the number of filter taps (similar to the YW-based AR model order).
3. Coefficients were computed by LMS and then used those coefficients to predict the next sample until the AR equation's prediction length.
4. Time-series forward prediction using the LMS-based AR model was calculated to predict 256ms (twice the length of 128 ms) (Figure 1, part C).

2.1.4 Performance Assessment of YW and LMS:

1. Means of the original and predicted data were computed and then subtracted their respective means from the original and predicted data.
2. The analytic signal was calculated using a Hilbert transform to calculate the instantaneous frequency and phase of the original and predicted data.
3. Then the phase difference was computed between the original and predicted data.
4. The phase locking value (PLV) was calculated between the original and predicted data segment in the final step.

The four steps of performance assessment are to be carried out for both YW and LMS methods. Figure 2 displays a flow chart depicting the whole algorithm.

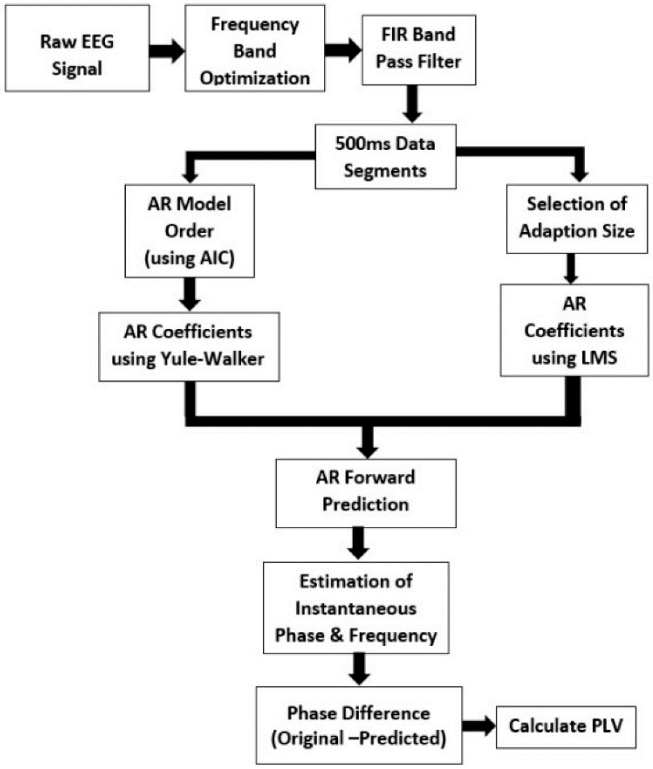

Figure 2 Overview of the Algorithm for Offline study. The flow chart represents sequential steps. The first four preprocessing steps and the last four assessment steps are identical for both the Yule-Walker (YW)-based AR model, and the least mean square (LMS)-based AR model.

2.2 Participants

Twenty-one healthy participants (10 males and 11 females; mean age ± standard deviation (SD), 26.2 ± 7.1) volunteered and provided informed consent for this study's EEG analysis. Participants were given instructions for an eyes-closed resting state for EEG data recording, whereas the recording duration of EEG signals was three minutes. The study was directed as per the Declaration of Helsinki and was approved by the RIKEN's ethics committee (Wako3 26-24). The EEG used in this study was also used in our earlier studies [47-49].

2.3 EEG Recording and Preprocessing

To record EEG signals at a 1000 Hz sampling rate, a 63-channel EEG cap ("Easycap, EASYCAP GmbH, Herrsching, Germany") and an EEG amplifier ("BrainAmp MR+, Brain Products GmbH, Gilching, Germany") were used. EEG amplifier's online low and high cutoff frequencies were fixed to 0.016 and 250 Hz. The 10/10 system was used for electrode positioning; the left earlobe was used to place the reference electrode, and AFz acted as the ground electrode. Re-referencing the EEG signals was done by averaging the left and right earlobes, followed by offline downsampling to 500 Hz. All analysis for the offline study was done in MATLAB ("Math-Works Inc., Natick, MA, USA") through EEGLAB [50] and customized scripts.

2.4 Statistical Analysis

MATLAB and the Statistics and Machine Learning Toolbox were utilized to carry out all statistical analyses. For this, $p<0.05$ was set as the level of statistical significance.

3 Results

The offline study's main goal was to assess the performance of an adaptive LMS model and a conventional YW model for time series forward prediction. We divided the results into three subsections: Time-series forward prediction for shorter length, Time-series forward prediction for twice length and for single channel O1 sampling points crossing the significant line.

3.1 Phase Locking Value

"Given two signals, for example, c and d with a frequency f, the technique calculates a measure of phase-locking amongst the elements of c and d for each latency at frequency f (this measure is known as a phase locking value or PLV)" [51]. Also, the PLV often categorizes phase synchronization between two signals.

In an offline study, both methods' performance at different time points was determined by the PLV [51]. The difference between the original and the predicted data segments' instantaneous phases was calculated, as displayed in Figure 3. This measure results in a numerical value between 0 and 1: zero indicating the large variation in phase, while one indicating trials having a similar phase.

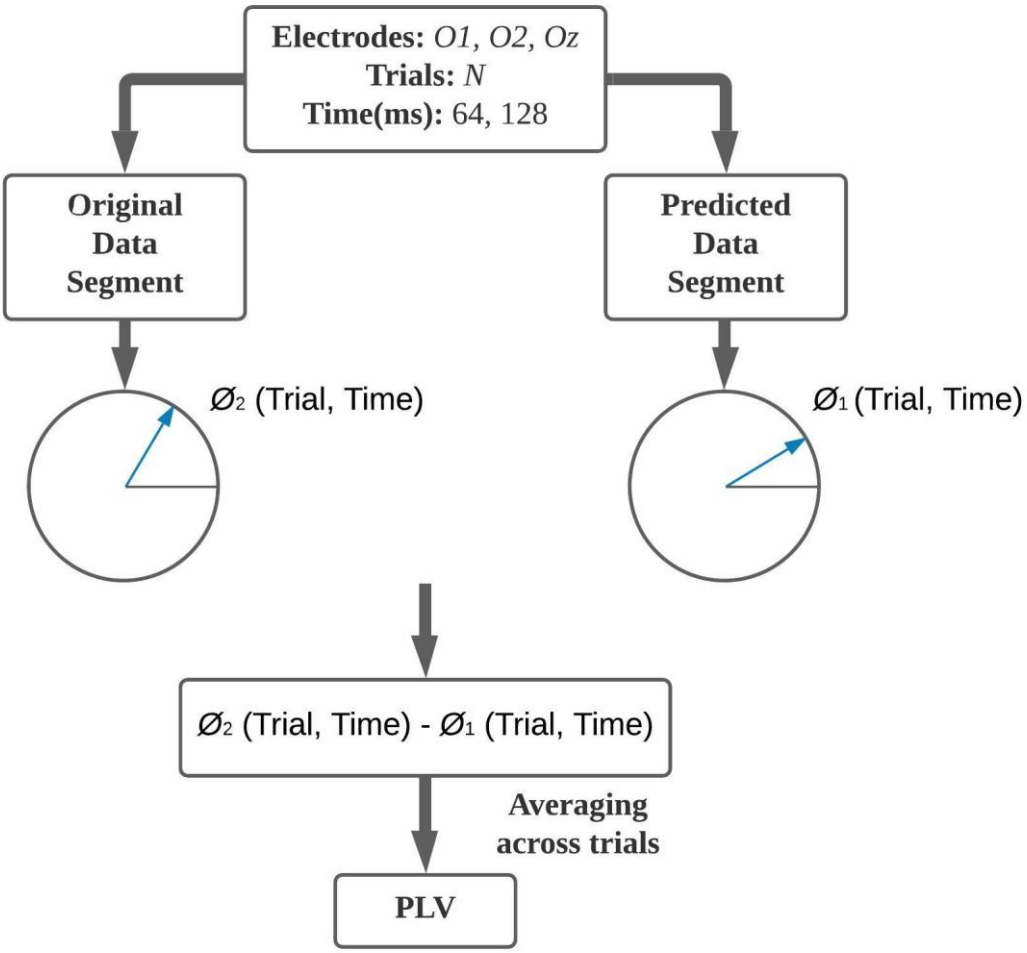

Figure 3 Phase-locking value (PLV) calculation method [51] between original and predicted data. For the same electrode, variations of phase differences between the predicted and original data within trials were evaluated. PLV was determined at three time points 0, 128, 256 ms, and three electrodes, O1, O2, and Oz.

3.2 Shorter Prediction Length

Comparing both methods at time points, 64 ms and 128 ms for three channels, O1, O2, and Oz were done using a paired *t*-test. And the mean Rayleigh's Z value (PLVrz) of all the participants are shown in Figure 4. The YW method's PLVrz values are shown in part A while part B reveals the LMS method's values. The values of PLVrz decreases gradually, signifying the decay of prediction performance with time. A significant difference was shown at 128 ms between the two methods indicating YW performs well compared to the LMS-based AR model. Around 700 trials, PLVrz > 2.9957 is deliberated statistically significant for the $p < 0.05$ significance level among twenty-one participants.

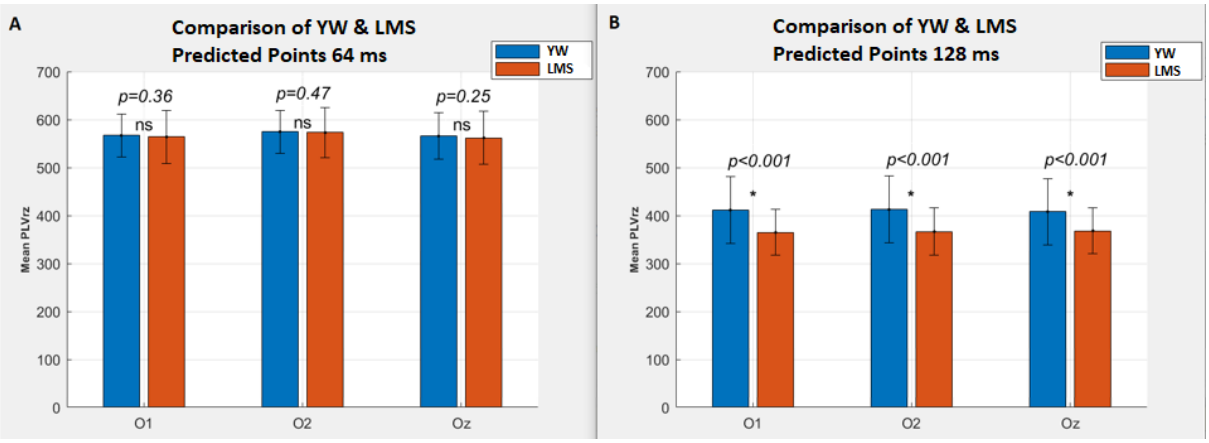

Figure 4 Rayleigh's PLV for the YW and the LMS-based AR model. ns denotes not significant *p*-value, whereas Asterisk (*) specifies a significant *p*-value. Part (**A**) shows the mean of Rayleigh's *Z* value (PLVrz) at the current time point (64 ms); Part (**B**) shows the mean PLVrz at 128 ms. Error bars indicate the standard deviation of the mean. YW is shown in blue color, and red color shows the LMS-based AR model.

3.3 Twice Prediction Length

The prediction length was doubled (from 128ms to 256ms (128 samples)) to examine how both methods perform competently. The prediction performance generally declines over time [52]. The LMS method indicated superior prediction performance with an increased length, as displayed in Figure 5.

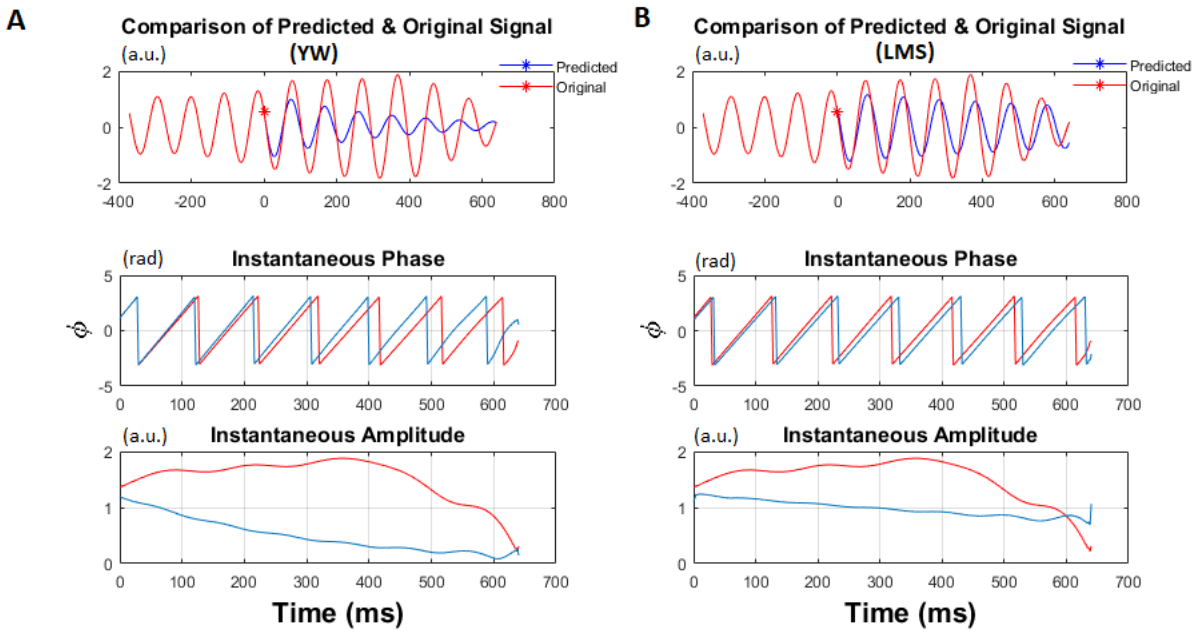

Figure 5 Representative prediction data of the YW-based AR model and the LMS-based AR model for twice the prediction length (256 ms). The red signal shows an original data segment, while the blue color indicates the predicted signal. Part (**A**) shows the instantaneous phase and amplitude of the YW-based AR model; Part (**B**) shows the LMS-based AR model and its corresponding instantaneous phase and amplitude. Asterisk (*) indicates the prediction starting point.

Representative values of PLVrz as a function of predicted time points for three different channels, O1, O2, and Oz, are shown in Figure 6. Both parts A and B of the figure show a decline for an increase in prediction length and crossing the significance line shown in red color. For this specific participant, the YW shows the 378 ms for crossing the significant line, while the LMS illustrates the 416 ms for crossing the significant line.

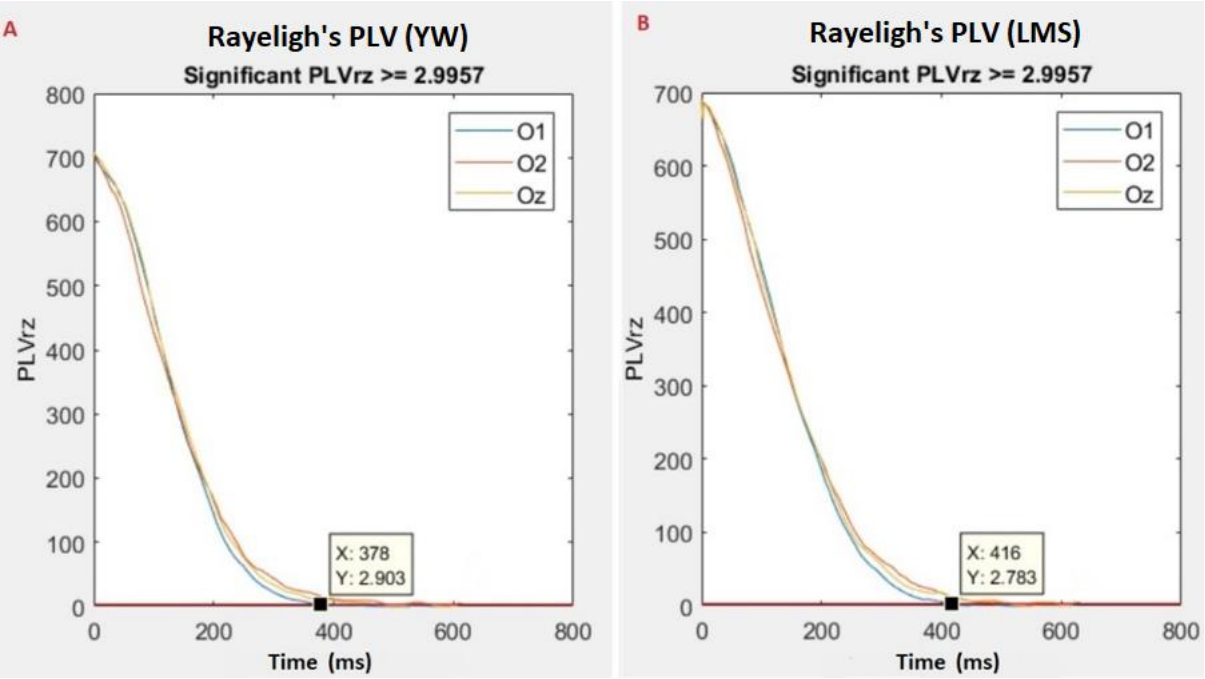

Figure 6 Rayleigh's Z value (PLVrz) for twice the prediction length (256 ms). (**A**) shows the AR model; (**B**) shows the LMS-based AR model. The red line indicates the significance level with a value of 2.9957. The box shows the time point (X-axis) at which the significant line is crossed with its respective PLVrz value (Y-axis).

Comparison between both methods was made using a paired *t*-test for all the three channels O1, O2, and Oz. For both prediction points, 128 ms and 256 ms, the LMS-based AR model showed greater PLVrz than the YW-based AR model. Even though both methods' performance dropped with an increase in the prediction length, the LMS-based AR model excelled the YW when the length was increased twice, as depicted by their mean PLVrz values in Figure 7.

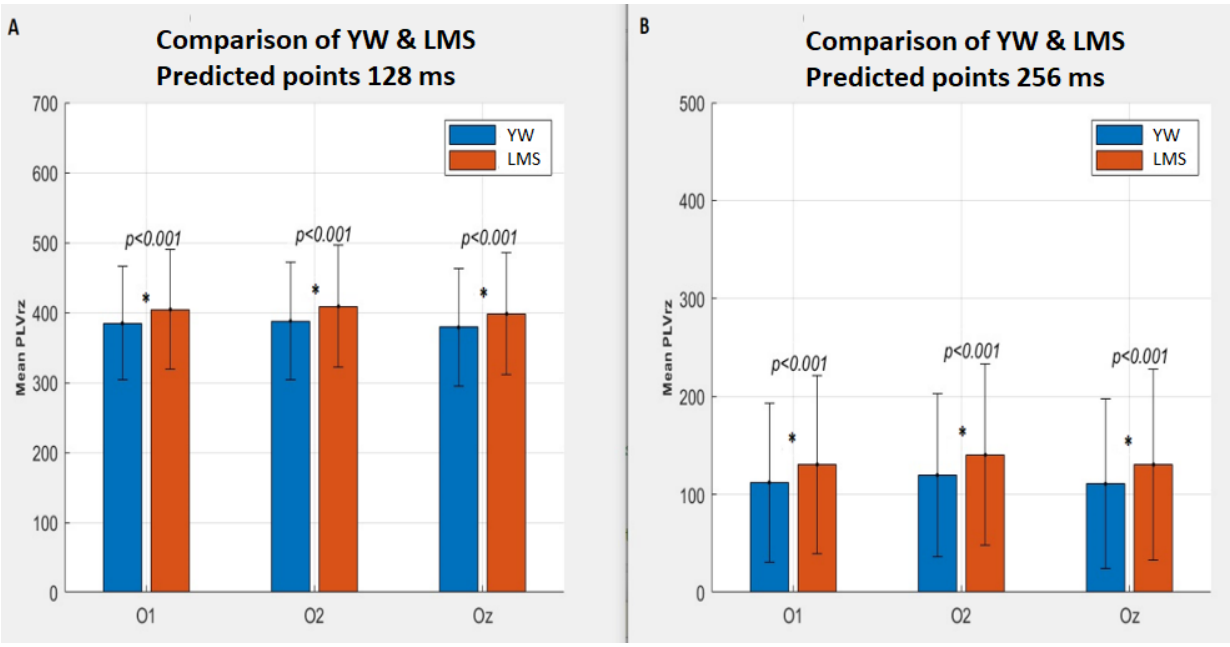

Figure 7 Statistical Comparison for the twice prediction length (256ms) between the YW-based AR model and the LMS-based AR model. Asterisk (*) shows a significant p-value. (**A**) Mean PLVrz at 128 ms; (**B**) Mean PLVrz at 256 ms. Error bars indicate the standard deviation of the mean. YW is shown in blue color, whereas the red color depicts the LMS-based AR model.

3.4 Sampling Points of Channel O1 Crossing the Significant Rayleigh's Z Value

In this part, we examined each participant's sampling points in the 800 ms interval and crossed the significant Rayleigh's Z value (>2.9957). With the increase in prediction length to 800 ms, both methods' performance decayed, as shown in Table 1. Among the 21 participants, 15 showed higher crossing values with the adaptive LMS-based AR model compared with the conventional YW-based AR model. For time points < 400, a significant difference was seen between the two methods, as depicted in Table 2.

At 64 ms (32 samples), the YW excelled the LMS, whereas, for the 128 ms, 256 ms, and 340 ms, the LMS-based AR model surpassed the conventional YW. For samples greater than 200 (400 ms), both methods' performance declined, and there was no significant difference among the two methods.

Table 1 Time points crossing the significant Rayleigh's PLV for channel O1 for both the Yule-Walker (YW)-based autoregressive (AR) model and the least mean square (LMS)-based AR model. Asterisk (*) indicates that out of 800 ms, the particular participant did not cross the significant value (>2.9957).

Participants	**Channel O1, for 800 ms prediction**	
	YW	**LMS**
	Time Points	**Time Points**
1.	424	446
2.	368	392
3.	536	550
4.	492	484
5.	382	416
6.	420	578
7.	452	456
8.	678	752
9.	392	370
10.	694	*
11.	630	678
12.	506	556
13.	702	618
14.	524	522
15.	796	*
16.	644	598
17.	528	578
18.	*	778
19.	566	598
20.	660	714
21.	452	406

Table 2 Statistical comparison of Rayleigh's Z value for 800 ms prediction of channel O1.

Prediction Time Point (ms)	***p*-value**	**YW**	**LMS**
		Rayleigh's *Z* Value (PLVrz) Mean Values	
64	$p < 0.001$	582	568
128	$p < 0.001$	384	403
256	$p < 0.001$	113	131
340	$p = 0.010$	50.5	61.18
400	$p = 0.070$	29	35

4 Discussion

Phase estimation of EEG rhythms is quite intricate because of the dynamic nature and low signal-to-noise ratio (SNR). The offline study proposed an adaptive approach for the estimation of the alpha oscillations phase. Our goal comprises facilitating EEG applications in real-time, relying on phase estimation. The offline study's main aim was to implement a time-series forward prediction using an adaptive LMS-based AR model and YW-based AR model.

In the offline study, the suggested adaptive method evaluates the instantaneous phase and instantaneous frequency of EEG data (alpha oscillations only, channels: O1, O2, and Oz) followed by signal prediction utilizing the abovementioned models. The performance assessment was done using PLV for two different prediction lengths (128 ms and twice of first length (256 ms)) of the EEG data. Earlier, Zrenner [20] implemented the YW-based AR model [19]. We implemented the AR model with the identical FIR bandpass filtering, AR model order, forward prediction length, and EEG data segment's original length for consistency as well as comparison. Moreover, we evaluated how the performance of both methods affected the future prediction window. In order to obtain the phase and frequency information from the EEG signals, complex wavelet transform [53], and the Hilbert–Huang transform [54, 55] was employed by earlier studies. Still, there is a limitation in applying these methods due to predicting non-stationary data's future. Though the conventional YW-based AR model can solve the EEG time-series' prediction, it presumes signals' stationarity over a certain period. Therefore, it is less suitable for closed-loop real-time applications for non-stationary time-series data, for instance, EEG. Conversely, to cope with the non-stationarity of EEG signals, our proposed adaptive method relies on recurrent updates, so predicting the signal in the future whereas adapting to changes dynamically.

Applying neurostimulation in a closed-loop scenario has increased considerably in the past decade, including the precise and accurate phase estimation of an ongoing neural oscillation. A previous study [56] used Hilbert transform- and Fast Fourier-based procedures for phase-synchronized stimulation in diverse EEG rhythms. This study suggested a short prediction algorithm with diverse windows for phase prediction and extraction based on intermittent protocol. Like our study, performance evaluation was done utilizing PLV as a performance metric, which exceeded a value of 0.6 for detecting the alpha band. Likewise, they also showed a decline in performance with the increase in prediction length in both approaches. The substantial shortcomings were negligence to demonstrate the closed-loop system's working entirely and small sample size. Another study described three techniques for predicting the phase (zero crossing, AR model-based, and Hilbert-based method) [52]. The performance was

evaluated utilizing different metrics like entropy-based phase synchrony, PLV, and degree deviation. This study also established that PLV declines when the time-window is increased and at lengthier intervals, as shown by the increase in alpha fluctuations. This research's limitations include failure to determine the optimal method among Hilbert-based and AR, a relatively small sample size of eight subjects and using only one channel Oz.

Standard signal processing techniques are used in most studies to estimate the phase. An interesting research showed machine-learning techniques for estimating the instantaneous phase of only one EEG signal (POz) [23]. Analogous to our offline study, they also carried out individual alpha frequency based frequency band optimization. The algorithm was divided into two parts to construct an analytic signal: on the former path, data was only epoched for generating an input signal, while on the latter part, a band-pass filter (FIR) was carried out on the data segment to create an output signal. The Hilbert transform and epoching accompanied the latter pathway as the final step before assessing the model. An optimized filter trained the data; Hilbert transform recovered the instantaneous phase and minimized MSE non-causal filtering. The main drawback of this process is the requirement for initial data preceding the main experiment for training. The offline analysis goal in our work was to evaluate the phase of an EEG data segment via an adaptive method. Supported by former studies, our findings demonstrate that the LMS-based AR model surpasses the YW-based AR model to predict long intervals. Also, for the O1 channel only, the LMS-based AR model specifies more samples above the significant line.

5 Conclusions

Our EEG phase estimation technique depends on instantaneous alpha oscillations utilizing the conventional YW and the adaptive LMS method. An adaptive LMS-based AR model's two primary purposes include: First, the adaptive method does not depend on familiarity with the exact stochastic signal, which is hardly accessible in reality. Second, it tracks the deviation in the EEG signal by dynamically adjusting its coefficients. Our study indicated that the adaptive method outperforms the conventional one in offline analysis for longer prediction lengths by comparing YW and LMS. This novel implementation may lead to EEG instantaneous phase prediction with low computational cost and produce versatile applications in basic and clinical neurosciences, like EEG phase estimation assists in BCIs.

PART III

REAL-TIME CLOSED-LOOP SYSTEM

6 Methodology

6.1 Implementation of a Closed-Loop System

We propose an experimental setup that prolongs current approaches by closing the loop between EEG signals (representing the instantaneous brain state) and visual stimulation. The visual stimulation timing is coupled to the online-detected instantaneous phase of the EEG alpha-band signal (peak and trough phases). Figure 8 presents an implementation of a real-time closed-loop system. EEG signals are acquired using an ActiCap Slim ("BrainProducts GmbH, Gilching, Germany") electrode system. A 24-bit 32-channel Tesla EEG amplifier ("NeurOne; Bittium Biosignals Ltd., Kuopio, Finland") is used for the EEG recordings, with data recorded in AC mode at a 20 kHz sample rate for succeeding analysis. The amplifier's analog output device is organized to reconstruct a filtered and an amplified analog signal from a set of 16 amplifier channels covering the occipital cortex selected by the user. Of the channel subset, O_z is analyzed utilizing a real-time system. A MATLAB experimental control scripts PC is attached to the "Performance real-time target machine" ("Speedgoat GmbH, Liebefeld, Switzerland"), which receives input signals from a 24-bit analog input module (IO109) and sends transistor-transistor logic (TTL) signal output to a digital output module (IO203 with 64 TTL channels). The digital output module further sends the TTL trigger signal from the "Performance real-time target machine" to the NeurOne Model Black High (Bittium Biosignals Ltd., Kuopio, Finland) referred to here as Trigger A. An additional 8-bit trigger is simultaneously sent from the "Performance real-time target machine" to the visual stimulus generating PC via serial port (RS232), which further sends it to the NeurOne Model Black High for subsequent data analysis. A real-time data acquisition system (Figure 8, part b) utilizing a Performance real-time target machine runs in parallel on a dedicated Target PC (SN4200, IO10; Speedgoat), digitally processing and logging the raw EEG data through the implementation of a Simulink real-time model (MathWorks Inc., Natick, MA, USA, 2018a) for each scenario (YW peak and trough, LMS peak and trough). The time lag due to the Performance real-time target machine is approximately 10 ms, while the time lag due to the NeurOne is about 4 ms.

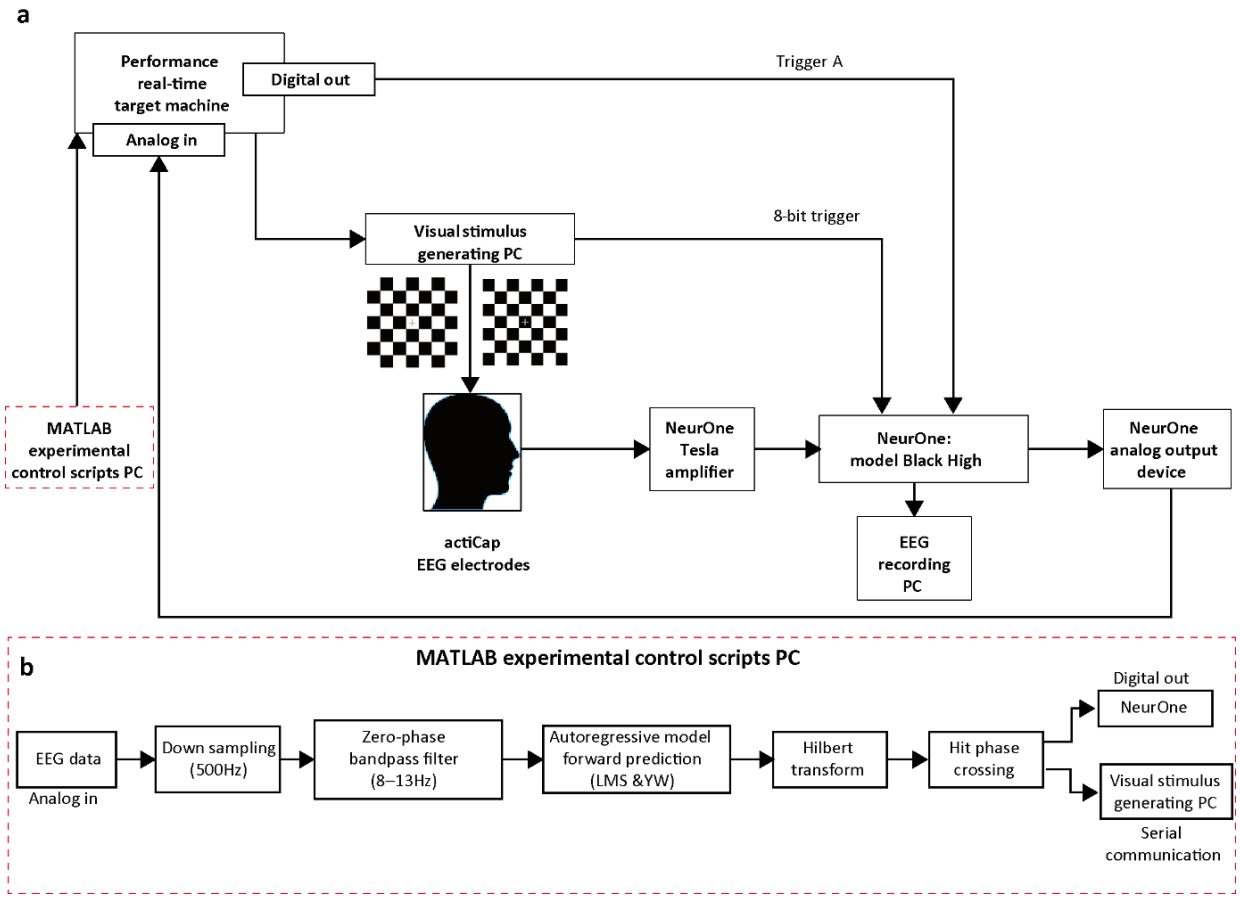

Figure 8 A schematic diagram of the real-time closed-loop system. (**a**) shows an implementation of a closed-loop brain state-dependent visual stimulation setup comprising electroencephalography (EEG), real-time signal processing, and triggered visual stimulation setup comprising electroencephalography (EEG), real-time signal processing, and triggered visual stimulation. The visual stimulation is locked to the instantaneous phase of the recorded EEG signal in the alpha band either at the peak or the trough. (**b**) shows sequential steps for time-series forward prediction implemented through MATLAB experimental control scripts PC via four distinct Simulink real-time models (Yule–Walker (YW) peak, YW trough, least mean square (LMS) peak, LMS trough). Raw EEG data were downsampled first, followed by finite impulse response (FIR) bandpass filtering. Coefficients of the autoregressive (AR) models were calculated, and the EEG signal was forward predicted. After time-series forward prediction based on YW/LMS methods, the instantaneous phase (at time-zero") was estimated using Hilbert transform. The visual stimulation was then triggered when a pre-set phase (peak or trough) condition was met.

6.2 Algorithm

The ultimate goals of this study were the real-time phase estimation of alpha rhythms and phase-dependent triggering. The instantaneous phase prediction algorithm can be divided into four parts: YW peak prediction, YW trough prediction, LMS peak prediction, and LMS trough prediction. Each part was further divided into the following sequential steps, except for step 4, which differs between the YW-based and LMS-based AR models. A distinct Simulink real-time model was designed for each of the four methods and implemented in the Performance real-time target machine.

1. In each Simulink model, the raw EEG data are received as analog input via IO109 with a sample rate of 2 kHz and are downsampled to 500 Hz.
2. The data are then delayed by 500 samples, and the mean of the data is calculated and subtracted from the original data. The data are then sent to the next step for filtering.
3. The third step implements bandpass filtering. A two-pass FIR bandpass filter (filter order 128, 8–13 Hz) is applied to the data, after which the edges are removed.
4. The fourth step is forward prediction. After trimming 85 samples from both sides, the remaining 330 samples are then used for forward prediction (85 samples). The YW forward prediction algorithm predicts the future. It computes coefficients using Yule-Walker equations, whereas the LMS forward prediction algorithm uses an adaptive method to compute coefficients and then uses them in the AR equation. This step results in a predicted signal as an output. The model order for both methods is 30.
5. The Hilbert transform is performed on resulting forward-predicted EEG data to determine the instantaneous phase at "time-zero".
6. The zero-phase crossing (a predetermined phase is crossed, with 0 and pi rad portraying positive and negative peaks, respectively) is monitored online, and a TTL signal is sent from the Performance real-time target machine via digital output module (IO203) and serial port (RS232). The Performance real-time target machine sends the TTL signal to the EEG recording PC via IO203, while the TTL signal is sent via RS232 to the visual stimulus generating PC simultaneously.

6.3 Participants

A total of nine volunteers (three males and six females; mean age 32.1 years ± 6.6 (SD)) with normal or corrected-to-normal vision were recruited to this study and provided informed consent for the EEG experiments. The ethics committee of RIKEN permitted the study. Data from the first three participants were recorded using the Tesla amplifier's DC mode, while data from the rest of the participants were recorded using the AC mode. The participant data recorded using the DC mode was noisier than that recorded using the AC mode, which resulted in relatively low amplitude output signals. The AC mode has a greater SNR than the DC mode and uses a 0.16 Hz low pass filter, leading to higher amplification of data for subsequent analysis. The SNR highly affected the prediction accuracy, and therefore only the participant data collected using the AC mode were used for further analyses. A spectral analysis was done on the remaining six participants to estimate the power in the alpha rhythm range (8–12 Hz).

6.4 Experiment

The experiment incorporated visual stimulation blocks and eyes-open resting blocks. Participants were requested to prevent eye blinks, eye movements, and jaw clenching. The whole experiment was divided into two sessions, each with ten blocks presented in random order, with these ten blocks consisting of five resting and five visual blocks. In both sessions, the ten blocks were linked with conditions, namely Resting, Visual Random, Resting YW (peak, trough), Resting LMS (peak, trough), Visual YW (peak, trough), and Visual LMS (peak, trough), as shown in Figure 9 (part a). Results were analyzed from blocks 2-5 and blocks 7-10. The total experiment took 1 hour and 10 minutes, including small breaks between blocks. For the resting condition, there were 90 trials for each block, while for the visual stimulation condition, there were 108 trials, as shown in part c of Figure 9. The visual experiment consisted of normal trials and response trials. The visual stimuli were shown on an liquid crytal display (LCD) monitor ("BenQ XL2420; BenQ Corporation, Taipei, Taiwan; refresh rate: 144 Hz; resolution: 1920 × 1080"), with a chin rest placed 100 cm from the monitor being used to maintain head position. The checkerboard stimuli (visual angle of 8.8°) consisted of 49 black-and-white squares (7 by 7) along with a fixation cross at the midpoint. The grids' color was temporally modified between black and white (luminance of black: 9.18 cd/m^2; white: 152.2 cd/m^2). The fixation cross was colored gray in regular trials and red in response trials. Participants were trained to click the left mouse button the moment a red fixation cross appears. The visual and resting tasks were implemented using NBS Presentation Version 20.0 ("Neurobehavioral Systems Inc., Albany, CA, USA"). Additionally, EEG signals were also measured for the resting scenario. At the same time, participants rested with their eyes open, seeing passively at the fixation cross presented at the midpoint of the screen part b Figure 9.

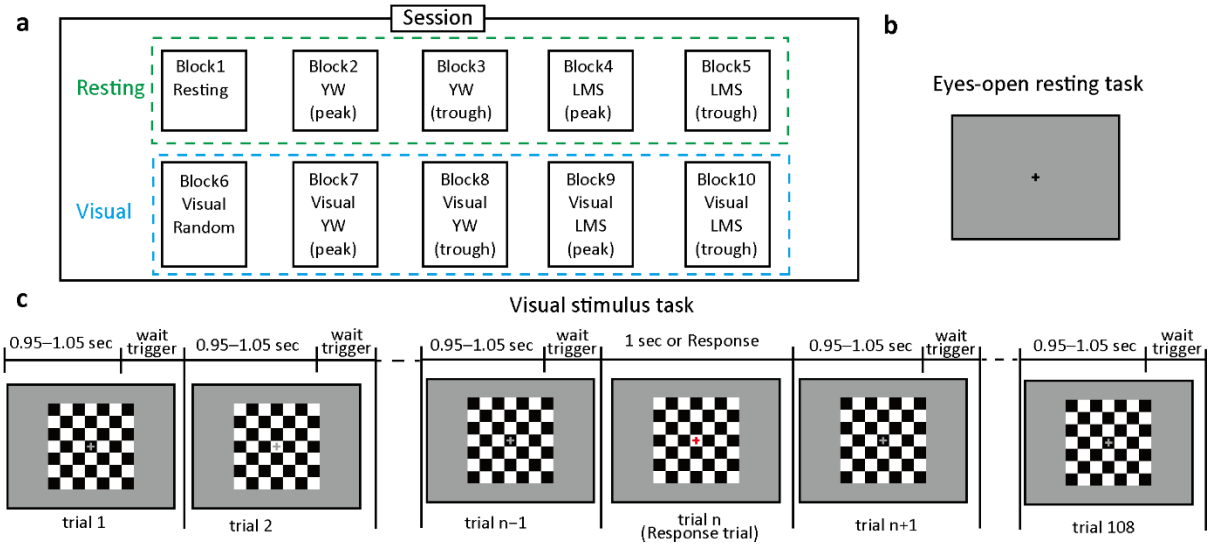

Figure 9 Overview of the experimental sessions and trials. Part (**a)** shows a session divided into resting (green) and visual (blue) parts, each with five blocks. "Peak" means a positive peak or 0 rad, while "trough" depicts a negative peak or pi rad. Part (**b)** shows an eye-open resting condition. Part (**c)** shows trials of the visual stimulus condition. Response trials are conducted with a red fixation cross at the center. Each trial took an average of 1.05 s.

6.5 EEG Recording and Preprocessing

The 63-channel EEG signals were recorded at 20 kHz of sampling rate using a Tesla amplifier and ActiCap slim EEG cap. Online low and high cutoff frequencies for the EEG amplifier were selected to 0.16 Hz and 3500 Hz, respectively. Electrodes were positioned according to the 10/10 system, with electrode AF_z as the ground electrode and the left earlobe as the reference electrode. EEG signals were re-referenced to the right and left earlobe's average and downsampled to 500 Hz for offline analysis. Only the downsampled signal was used to calculate the phase-triggered response (PTR). In contrast, for the PLF and instantaneous phase calculation, a two-pass FIR bandpass filter (8–13 Hz) with a filter order of 128 was applied to the EEG signals. All analysis was done in MATLAB R2018a using EEGLAB [50] and a personalized script.

6.6 Statistical Analysis

All statistical analyses were done using MATLAB and the Statistics and Machine Learning Toolbox, with $p<0.05$ being set as the level of statistical significance.

7 Results

7.1 Phase Locking Factor

"The phase locking factor (PLF) assesses whether the difference between the oscillators' phases is strongly or weakly clustered around some angle in the complex unitary circle" [57]. The PLF was defined as follows:

$$PLF = \frac{1}{N}\left|\sum_{n=1}^{N} e^{j\theta_n}\right|, \qquad (10)$$

where θ_n is the instantaneous phase at "time-zero" for the *n*th trial, and *N* represents the total number of trials. A PLF closer to zero indicates high phase variability over trials, while a PLF closer to 1 depicts all trials as owning a similar phase. It should be noted that the phase variance is 1-PLF [57].

The Rayleigh test can verify the statistical significance of the PLF to calculate ZPLF [14, 57], which is Rayleigh's Z value computed using PLF as follows:

$$ZPLF = N(PLF)^2. \qquad (11)$$

To measure the statistical significance of the participant-averaged ZPLF values, the value was corrected to $ZPLF_{all}$:

$$ZPLF_{all} = \frac{1}{\sqrt{P}}\sum_{p=1}^{P} ZPLF_m, \qquad (12)$$

where *P* depicts the number of participants [58].

Towards the evaluation of the difference between YW and LMS within each participant, we also examined Watson's U^2 test for each of the two conditions (resting and visual), according to the method proposed by Persson [59]. If the calculated U^2 is larger than the critical value, the two sample circular distributions differ significantly from each other. For the current study, the critical value $U^2(\infty, \infty; p<0.05) = 0.187$. As this test contrasts both the phase variance and the average of the phase angular data, the effects of the difference in average phase angles were removed by shifting the phase according to the following [60]:

$$\boldsymbol{\theta_{new}} = \boldsymbol{\theta} - \varphi, \qquad (13)$$

$$C = \frac{1}{N}\sum_{n=1}^{N}\cos\theta_n, \qquad (14)$$

$$S = \frac{1}{N}\sum_{n=1}^{N}\sin\theta_n, \qquad (15)$$

where $\boldsymbol{\theta}$ is the vector of instantaneous phases at zero ms, $[\theta_1, \cdots, \theta_N]$, $\varphi = tan^{-1}(\mathrm{S/C})$, and $\boldsymbol{\theta_{new}}$ are used in the calculation of Watson's U^2 test.

Using this transformation, we can compare the differences in phase variance between the two circular distributions.

7.2 Phase-triggered response (PTR)

PTR is defined as the grand-average of triggered EEG signals from distinct trials within each participant.

$$PTR(s) = \frac{1}{N}\sum_{n=1}^{N} S_n(s), \qquad (16)$$

where S_n represents the downsampled EEG signal for the *n*th trial as a function of the sample point *s* within each trial extracted based on the trigger at "time zero" generated by the phase prediction methods. *s* ranges between 0 to 1000 centered around "time-zero", *N* is the total trials for each participant.

PTR is calculated in a similar manner to event-related potentials (ERP). Still, it doesn't depend on the external stimulus (namely visual or auditory stimuli) and uses a generated trigger based on the EEG phase. It is a measure for checking the prediction performance.

To check both YW and LMS methods' performance, the PLF at "time-zero" was assessed in both resting and visual tasks.

7.3 Resting Condition

The results of ZPLF and PTR for the resting condition are shown in Figure 10. ZPLF and PTR are shown individually for the five participants. The bold black lines in Figure 10 a–d indicate $ZPLF_{all}$. For a number of trials > 60, a ZPLF > 2.995 (which is called the critical value) is considered statistically significant. $ZPLF_{all}$ is also statistically significant if it exceeds the critical value. The small square box on the $ZPLF_{all}$ line represents "time-zero." In parts a–d, $ZPLF_{all}$ crosses the critical value indicated as a dotted red line. We found that ZPLF and $ZPLF_{all}$ were statistically significant for all participants except for the YW trough condition in participant P01. Our findings accord with former studies showing a ZPLF decrease when time increases [37, 52]. Figure 10 e–h shows the PTR for individual participants. In the PTR plots,

the squares for “time-zero” are observed at the peak for the peak condition and the trough for the trough condition. The black bold lines show the mean PTR.

Rose plots for each participant are shown in Figure 11. For the peak condition, these rose plots show an accumulation of values toward 0 rad, while for the trough condition, the rose plots show an accumulation toward pi rad. The summarized results of PLF and ZPLF and their mean ± SD are shown in Table 3. The bold values indicate significantly higher ZPLF compared to a critical value of 2.995. Besides, the ZPLFs of all participants crossed the critical value at “time-zero”, except for the YW trough condition of participant P01, as shown in Figure 10c. Table 4 presents the mean angle in radians and Watson’s U^2 test results.

The bold values indicate where the calculated U^2 values are greater than the critical value, and the differences in the two-phase variances are statistically significant. For participants P01 and P02, the LMS trough performed better than the YW trough. For participant P03, the LMS peak performed better than the YW peak condition. For participant P04, the YW trough surpassed the LMS trough. No significant difference was shown in participant P05 indicating both YW and LMS methods performed equally at “time-zero”.

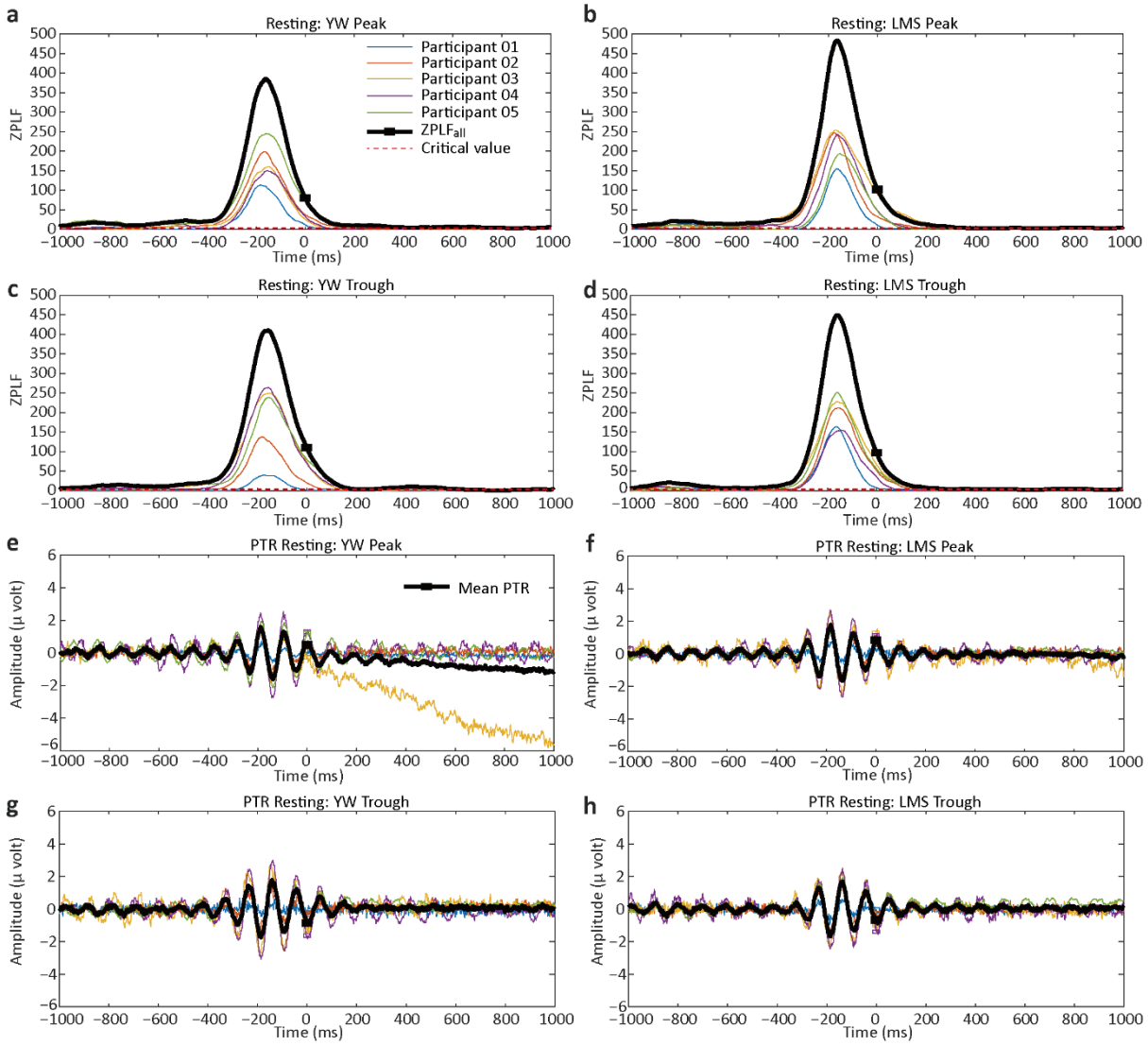

Figure 10 ZPLF and phase-triggered response (PTR) for the resting task for each individual participant. The bold lines depict $ZPLF_{all}$ or mean PTR. (**a**) ZPLF results for the YW method peak condition for the individual participants. (**b**) ZPLF results for the LMS method peak condition. (**c**) ZPLF results for the YW trough condition. (**d**) ZPLF for the LMS trough condition. (**e**) PTR for the YW peak condition. (**f**) PTR for the LMS peak condition. (**g**) and (**h**) PTR for the YW and LMS trough conditions, respectively. The black lines in e–h indicate the mean PTR across participants.

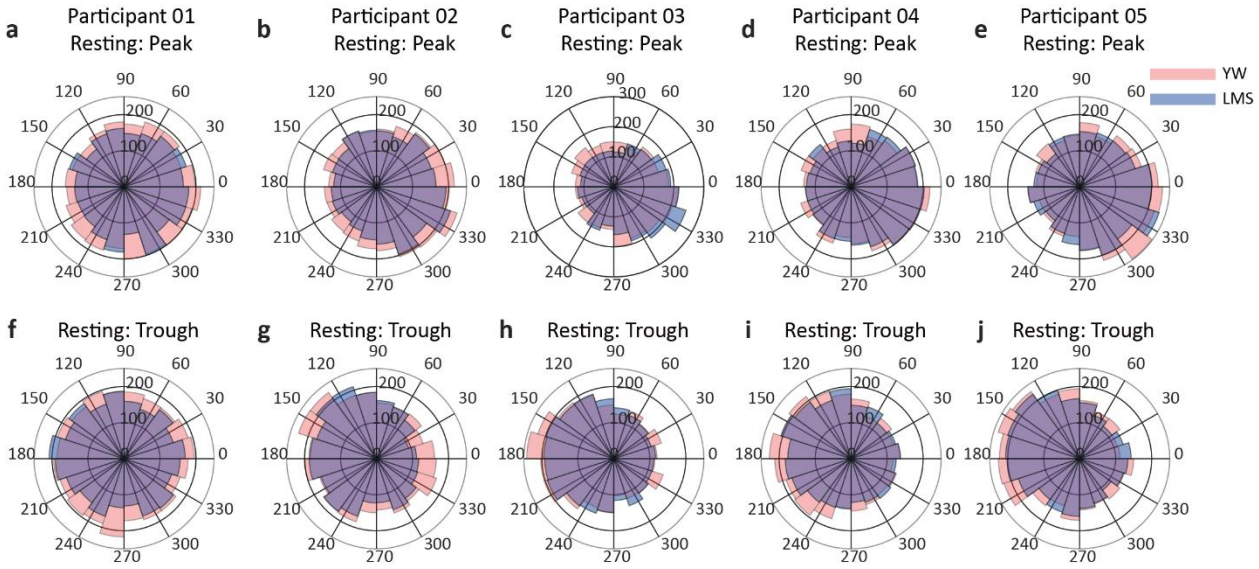

Figure 11 Rose plots for the resting conditions for each participant. The upper row (**a**–**e**) shows the rose plots for each participant's peak condition, while the lower row (**f**–**j**) depicts the rose plot for the trough condition for each participant. The peach color indicates the YW method, while purple indicates the LMS method. The violet color depicts the overlapping region.

Table 3 Overview of the results of the resting condition. The number of trials, PLF, and ZPLF at "time-zero" are shown.

Resting												
ID	**Number of Trials**				**PLF**				**ZPLF**			
	YW Peak	**LMS Peak**	**YW Trough**	**LMS Trough**	**YW Peak**	**LMS Peak**	**YW Trough**	**LMS Trough**	**YW Peak**	**LMS Peak**	**YW Trough**	**LMS Trough**
P01	3598	3156	3710	3276	0.057	0.059	0.019	0.047	**11.872**	**11.102**	1.432	**7.378**
P02	3491	3093	3433	3075	0.104	0.103	0.075	0.126	**37.831**	**32.895**	**19.778**	**51.678**
P03	3192	3038	3099	2993	0.090	0.171	0.155	0.149	**26.283**	**89.706**	**74.474**	**66.55**
P04	3230	3089	3268	3053	0.101	0.125	0.146	0.107	**33.569**	**48.528**	**70.241**	**35.50**
P05	3326	3159	3340	3139	0.146	0.122	0.155	0.133	**71.307**	**47.381**	**80.566**	**55.752**
Mean	3367.4	3107	3370	3107.2	0.100	0.116	0.110	0.113	36.172	45.922	49.298	43.371
SD	173.068	50.955	226.005	107.843	0.031	0.040	0.060	0.039	21.978	28.758	36.099	23.005

Table 4 Mean angle and Watson U^2 test results at "time-zero" for the resting condition.

Resting						
ID	**Mean Angle (rad)**				**WatsonU²**	
	YW Peak	**LMS Peak**	**YW Trough**	**LMS Trough**	**YW vs. LMS Peak**	**YW vs. LMS Trough**
P01	−0.475	−0.154	−3.009	2.580	0.059	**1.125**
P02	−0.228	−0.108	2.821	2.761	0.054	**0.273**
P03	−0.350	−0.369	2.923	2.956	**0.570**	0.099
P04	−0.271	−0.337	2.920	2.613	0.078	**0.207**
P05	−0.216	−0.333	2.872	2.827	0.887	0.064
Mean	−0.297	−0.260	2.961	2.747		

Taken together, the results suggest that we succeeded in outputting triggers targeting specific phases of alpha oscillations in a real-time implementation under resting conditions, doing this with both YW-based and LMS-based AR models.

7.4 Visual Condition

The results of ZPLF and PTR for the visual condition are shown in Figure 12. We observed two peaks in ZPLF for the visual condition, with the second peak corresponding to the visual response around 100 ms. The small black square in Figure 12 shows "time-zero". Rose plots for the visual condition are presented in Figure 13. For the peak condition, the rose plots are somewhat inclined toward the right side (0 degrees), but there is not an apparent inclination toward the left side for the trough condition. The YW and LMS troughs did not pass the critical line for participant P01, and the rose plots, therefore, do not show any leaning toward the left side. The summarized PLF, ZPLF, mean angle, and Watson's U2 test results for the visual task are shown in Table 5 and Table 6. All participants showed significant ZPLF values for each method and each condition. There was no significant difference statistically for any of the condition in participants P04 and P05. For participants P01 and P03, the LMS trough surpassed the YW trough, but for participant P02, the YW trough was better than the LMS trough, as shown by the bold Watson U2 test values.

The results suggest that we succeeded in giving visual stimulation targeting specific phases of alpha oscillations in a real-time implementation, doing this with both YW-based and LMS-based AR models. We observed the stimulation-induced brain responses.

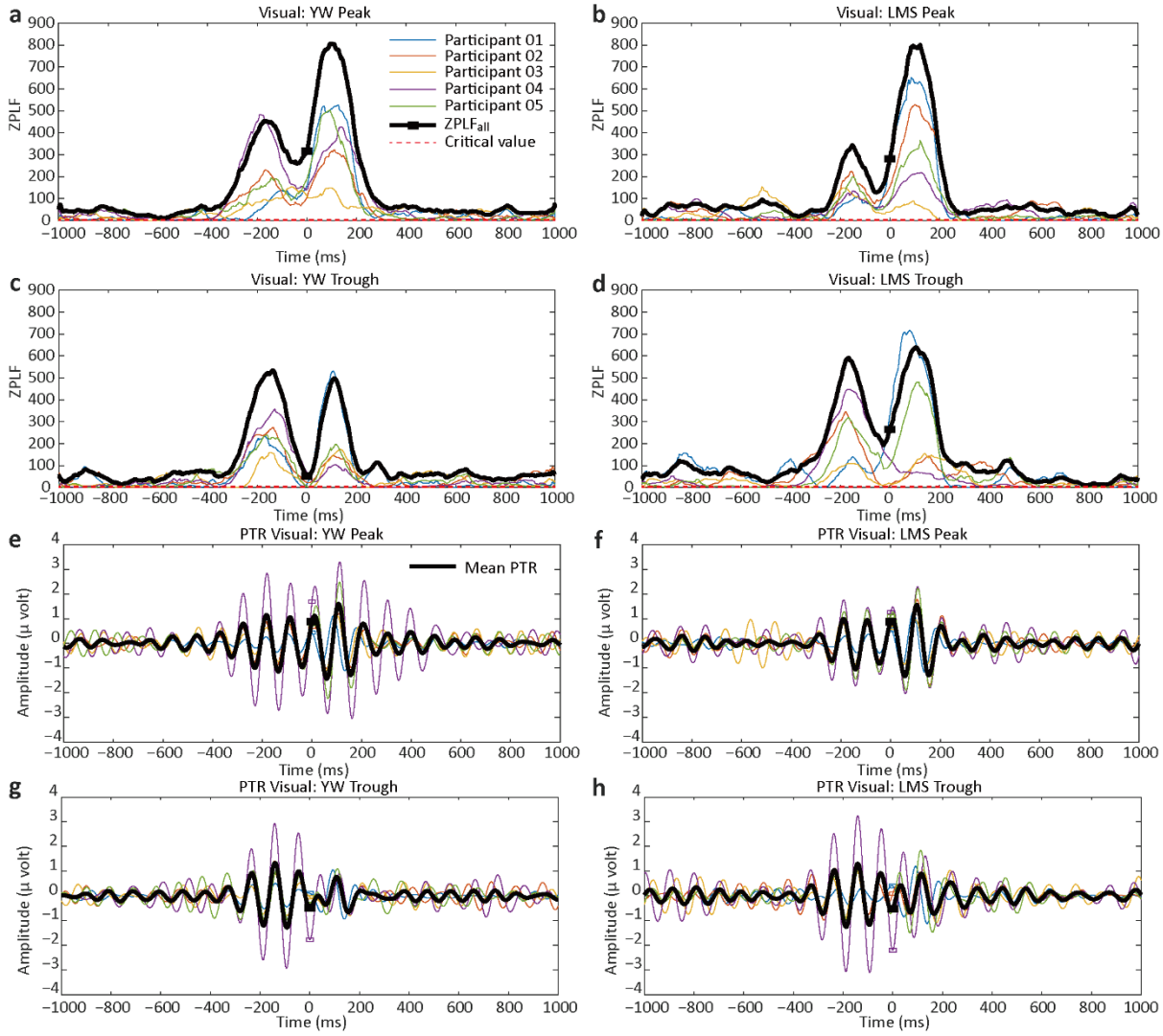

Figure 12 ZPLF and PTR for the visual task. Parts **a–d** show ZPLF results for both YW and LMS methods with peak and trough conditions, while Parts **e–h** show the phase-triggered response (PTR) for YW and LMS methods for the peak and trough conditions. ZPLF shows a second peak of around 100 ms for the visual task. The small black square shows "time-zero". The black bold signals in e–h show the mean PTR.

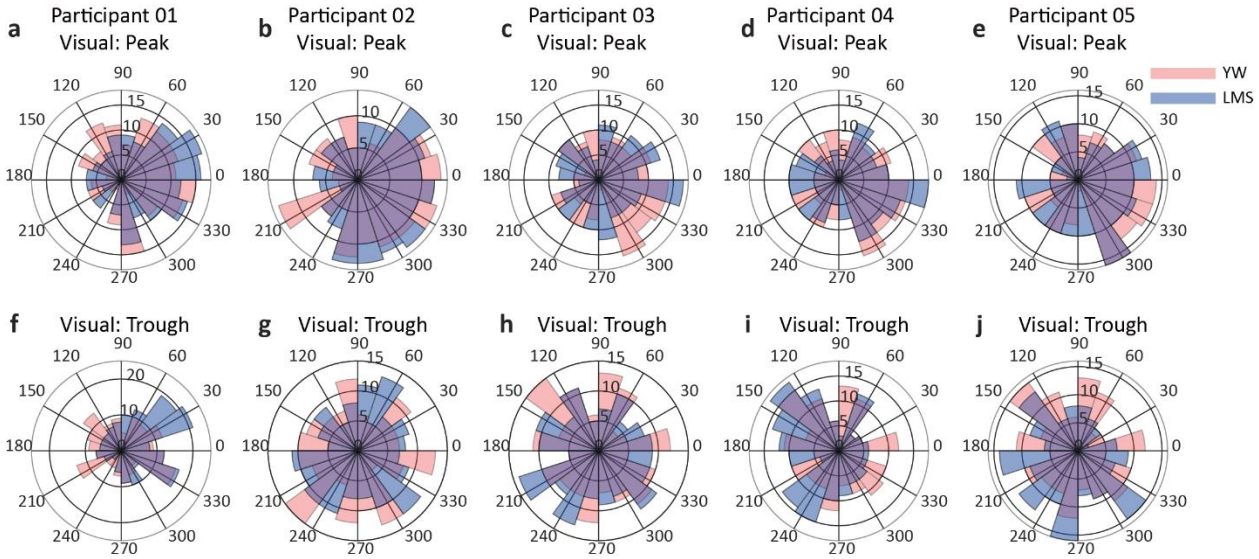

Figure 13 Rose plots for the visual condition. The participant's peak conditions are shown in the first row (**a–e**), while the trough conditions are depicted in the second row (**f–j**).

Table 5 Summary of the results of the visual condition. The number of trials, PLF, and ZPLF at "time-zero" are shown.

Visual												
ID	**Number of Trials**				**PLF**				**ZPLF**			
	YW Peak	**LMS Peak**	**YW Trough**	**LMS Trough**	**YW Peak**	**LMS Peak**	**YW Trough**	**LMS Trough**	**YW Peak**	**LMS Peak**	**YW Trough**	**LMS Trough**
P01	3780	3671	3788	3646	0.204	0.26	0.062	0.302	**158.5**	**255.8**	**14.760**	**333.35**
P02	3772	3553	3776	3575	0.166	0.20	0.078	0.047	**105.1**	**153.4**	**23.016**	**8.146**
P03	3630	3420	3760	3385	0.176	0.10	0.037	0.071	**112.7**	**39.50**	**5.326**	**17.461**
P04	3745	3762	3472	3461	0.194	0.15	0.141	0.193	**142.0**	**85.39**	**69.912**	**128.92**
P05	3774	3549	3776	3588	0.224	0.16	0.035	0.170	**190.2**	**93.69**	**4.871**	**103.98**
Mean	3740.2	3591	3714.4	3531	0.193	0.17	0.071	0.157	141.7	125.5	23.577	118.38
SD	63.057	130.4	135.870	105.624	0.022	0.059	0.043	0.102	34.72	83.34	26.962	131.21

Table 6 Visual condition results. The mean angle and Watson U^2 test results for the visual condition at "time-zero" are shown.

Visual						
ID	**Mean Angle (rad)**				**WatsonU^2**	
	YW Peak	**LMS Peak**	**YW Trough**	**LMS Trough**	**YW vs. LMS Peak**	**YW vs. LMS Trough**
P01	0.478	0.158	0.708	0.449	0.054	**0.338**
P02	−0.481	−0.407	−2.030	−1.090	0.031	**0.951**
P03	−0.169	−0.117	2.643	−2.112	0.046	**0.554**
P04	−0.655	−0.603	−2.810	−3.067	0.064	0.069
P05	−0.883	−0.657	−2.673	−2.167	0.093	0.151
Mean	−0.355	−0.327	−2.918	−1.882		

The summarized results of both resting and visual tasks regarding percentage and the total participants showing significant ZPLF are presented in Table 7. ZPLF value > 2.995 is considered to be significant. Significant ZPLF means that we achieved the desired result of outputting the triggers targeting a specific alpha oscillation phase. For the resting task, peak condition, all participants indicated significant ZPLF values for both methods. And for the trough condition, all participants showed the significant ZPLF for LMS, and only one participant did not show the significant ZPLF value for the YW method. The results indicate that all participants in both methods and all conditions crossed significant ZPLF values in the visual task. Overall, all the results specify that we succeeded in outputting the triggers targeting specific phases of alpha oscillations in a real-time implementation, doing this with both YW-based and LMS-based AR models except for one participant in one condition.

Table 7 Overview of resting and visual task results. Percentage and the total number of participants showing a significant ZPLF value for each condition.

Total Participants = 5	Resting				Visual			
	YW Peak	LMS Peak	YW Trough	LMS Trough	YW Peak	LMS Peak	YW Trough	LMS Trough
Participants	5/5	5/5	4/5	5/5	5/5	5/5	5/5	5/5
Percentage	100%	100%	80%	100%	100%	100%	100%	100%

8 Discussion

Utilizing EEG signals from channel Oz (occipital cortex), our research performed, for the first time, real-time EEG phase-dependent triggers for visual stimulation. These triggers were centered on a conventional YW-based AR model as well as a novel adaptive LMS-based AR model. The primary purpose was to consider and confirm the possibility of implementing a real-time closed-loop system based on the adaptive LMS-based technique, which we formerly suggested and established by studying offline data [37]. The online (proof-of-concept) study results provide empirical evidence that the adaptive technique is implementable in real-time. Individual differences were found in the closed-loop systems' performance, and results are presented at “time-zero” individually. In an eyes-open resting state, all participants indicated significant ZPLF for both techniques (peak and trough conditions), except for participant P01’s trough condition in the YW-based method. In the visual task, all participants presented significant ZPLF for each condition in both conventional and adaptive approaches. Both methods did equally, and the difference concerning any of the conditions was not statistically significant, as shown in the results of Participant P05. While there are individual differences in the EEG phases prediction, the proposed technique successfully outputted the stimulation triggers suggested by the results for most participants.

In our offline analysis [37], we indicated the advantage of our adaptive LMS-based method over the conventional YW-based method in phase prediction of alpha-band EEG. But, we could not show the dominance of the adaptive LMS-based method at "time-zero" because of the small number of participants, making it difficult to make a clear comparison. Although our primary focus was on implementing the adaptive method in real-time, one limitation of the online study arose from the EEG amplifier's DC mode's technical issues. Only five participants' data utilizing the AC mode were analyzed for the real-time closed-loop system. Hence, additional studies will need to elucidate the proposed adaptive method's superiority over the conventional non-adaptive method in a real-time implementation. Our results indicate that we achieved the desired results in measuring brain responses for triggered visual stimulation with a low computational cost. Even though our study involved visual stimulation only, other NIBS techniques such as TMS can be triggered using our adaptive method.

For estimating the phase, some former studies relied on machine learning techniques, and a variety of methods, mainly deep learning, were employed in BCI systems. To detect schizophrenia, a convolutional neural network (CNN) model with eleven layers has been utilized [61], leading to a classification accuracy of 98% for non-participants and 81% for the healthy and schizophrenic participants based testing. Regardless of great classification accuracy, the main shortcomings comprise a small data size; also, CNN's computation is expensive in comparison with conventional machine learning techniques. A system to detect parkinson's disease (PD) automatically also employed CNN with an accuracy of 88.25% [62]. For p300 EEG signals, a different study implemented principal component analysis (PCA)-based on CNN [63]. PCA was utilized for the signal's dimensionality reduction and decreasing the computational cost by keeping the original signal features. To improve EEG motor imagery signals' recognition rate, an amalgamation of the simplified CNN (SCNN) and continuous wavelet transform was applied [64]. Although the SCNN reduces the parameter and shortens the training time compared with CNN; but, the classification accuracy needs to be enhanced. The major drawback of such techniques is the requirement for initial data for training before the main experiment. In real-time phase estimation, the trained filters depend on signal quality and signal properties due to the absence of future information. Due to this, the technique fails to achieve unbiased phase estimation. Being highly proficient, deep learning still needs plentiful data for training and enormous processing power and are thus costly to implement. Conversely, our proposed adaptive method does not necessitate comprehensive training and computational cost.

We propose that our method be applied to fundamental neuroscience (such as neural oscillations' functional role) and clinical fields. In the past decade, considerable advancement has been done in invasive brain stimulation, dynamically responding to the existence of deviating neural activity [65, 66]. For instance, deep brain stimulation within a small PD patients group caused 30% clinical improvements approximately than a standard open-loop system [67]. When necessary, a device for closed-loop stimulation might send stimulation skillfully due to carrying out stimulation merely once brain function shows abnormal neural activity or damaged [68]. It also synchronizes every stimulus with the instantaneous brain state of the patient. Brain state-dependent stimulation has a therapeutic capability for brain disorders, for instance, schizophrenia, epilepsy, stroke, and PD. Future studies will include the implementation of the adaptive method in a real-time TMS-EEG system and the exploration of new scenarios for alpha and other oscillations.

9 Conclusions

In a real-time closed-loop system, we succeeded in implementing an adaptive as well as the conventional method. The real-time closed-loop system involves a time-series forward prediction and phase-locked visual stimulation. EEG triggered visual stimulation depending on brain-state was synchronized with the EEG peaks and troughs of alpha oscillations in both a resting state (open eyes) and a visual task. Our results showed that we succeeded in outputting triggers targeting specific phases of alpha oscillations in a real-time implementation, doing this with both YW-based and LMS-based AR models. Although our main focus was on alpha oscillations only, this real-time closed-loop system can also analyze other frequency bands. This novel implementation may lead to EEG instantaneous phase prediction with low computational cost and produce versatile applications in basic and clinical neurosciences, like EEG phase estimation assists in BCIs.

PART IV

CONCLUSIONS & FUTURE DIRECTIONS

10 Conclusions

In EEG, the instantaneous phase of neural oscillations is a brain state measure modulating evoked responses and linking neuronal processing. Nevertheless, phase estimation with standard signal processing techniques in the real-time closed-loop setup is difficult due to technical issues (such as SNR, fluctuations in EEG signal, complexity in computations, latency, jitter, artifacts, etc.) at the time of the stimulus. To calculate the signal's instantaneous phase, these techniques require data before and after the time of interest. Estimating phase in real-time or in the post-hoc scenario at the time of a stimulus, like a TMS pulse and potentials evoked by sensory stimulation in EEG, data availability is only before the time of interest. EEG signals are non-stationary, and for time-series forward prediction, conventional methods like YW compute coefficients of interest only once. Therefore, an adaptive method is required. The current study suggested an adaptive approach to estimate the instantaneous phase of alpha oscillations. The main objective was to implement a time-series forward prediction using the LMS-based AR model and YW-based AR model in a closed-loop system. To test and verify our proposed method and before source allocation, we divided the study into two parts, first instantaneous phase estimation of alpha oscillations offline and second, its implementation in a real-time closed-loop system.

- The offline study's suggested adaptive method evaluates the instantaneous phase and instantaneous frequency of EEG data (alpha oscillations only, channels: O1, O2, and Oz) followed by signal prediction utilizing the YW and LMS-based AR models. The performance assessment was done using PLV for two prediction lengths (128 ms and twice of first length (256 ms)) of the EEG data. Moreover, how the performance of both methods affected the future prediction window was also assessed. To cope with the non-stationarity of EEG signals, our proposed adaptive method relies on recurrent updates, so predicting the signal in the future whereas adapting to changes dynamically. Our findings demonstrate that the LMS-based AR model surpasses the YW-based AR model to predict long intervals. Also, for the O1 channel only, the LMS-based AR model specifies more samples above the significant line.

- The accuracy with which phase can be estimated differs more strongly within-subjects than between subjects; selection of the exact instant to stimulate may be essential than the selection of the right participant [21]. Oscillatory power being task-dependent, targetting a phase throughout a task can amplify the concerned oscillation. Utilizing EEG signals (channel Oz),

our research performed, for the first time, real-time EEG phase-dependent triggers for visual stimulation. These triggers were based on a conventional YW-based AR model as well as a novel adaptive LMS-based AR model. The main purpose was to check and confirm the possibility of implementing a real-time closed-loop system based on the adaptive LMS-based technique, which we formerly suggested and established by studying offline data [37]. The online (proof-of-concept) study results provide empirical evidence that the adaptive technique is implementable in real-time. Individual differences were found in the closed-loop systems' performance, and results are presented at "time-zero" individually. For the resting task, peak condition, all participants indicated significant ZPLF values for both methods. And for the trough condition, all participants showed the significant ZPLF for LMS, and only one participant did not show the significant ZPLF value for the YW method. The results indicate that all participants in both methods and all conditions crossed significant ZPLF values in the visual task. Overall, all the results specify that we succeeded in outputting the triggers targeting specific phases of alpha oscillations in a real-time implementation, doing this with both YW-based and LMS-based AR models except for one participant in one condition.

- Our results indicate that we achieved the desired results in measuring brain responses for triggered visual stimulation with a low computational cost and can be used as an alternative to the conventional approach.

11 Future Directions

Advancements in the modern closed-loops systems with small latency and small jitter are necessary to suit the multiple time-scales of the environment. This approach seems promising in developing a comprehensive closed-loop system in treating psychiatric and neurological disorders. There is substantial therapeutic as well as experimental potential in applying brain-state-dependent stimulation when the patient or participant simultaneously carries out a task. Therefore, future studies will include but not limited to:

- **Instantaneous amplitude**: in real-time, accuracy in the estimation of phase can be enhanced by comprising an instantaneous amplitude; therefore, assessing PTRs at high amplitude versus low amplitude responses can be tested.

- **Advantage of an adaptive method in real-time**: our offline study showed the adaptive method's advantage over the conventional one; additional studies will be required to reveal the adaptive method's superiority in a real-time closed-loop system.
- **Other neural oscillations**: Although our main focus was on alpha oscillations only, the offline and real-time closed-loop system can also analyze other frequency bands.
- **TMS-EEG setup:** implement the adaptive method in a real-time TMS-EEG system and explore new scenarios for alpha and other oscillations.
- **BCIs:** applications in basic and clinical neurosciences, like EEG phase estimation, assists in BCIs.
- **Deep learning:** checking the efficacy of the proposed method utilizing machine learning, specifically deep learning techniques.

12 Bibliography

1. Womelsdorf, T; Schoffelen, JM; Oostenveld, R; Singer, W; Desimone, R; Engel, AK; Fries, P. Modulation of neuronal interactions through neuronal synchronization. *Science*. **2007**, *316(5831)*, 1609-1612; https://doi.org/10.1126/science.1139597
2. Mathewson, K.E; Lleras, A; Beck, DM; Fabiani, M; Ro, T; Gratton, G. Pulsed out of awareness: EEG alpha oscillations represent a pulsed-inhibition of ongoing cortical processing. *Front. Psychol.* **2011,** *2*, 99; https://doi.org/10.3389/fpsyg.2011.00099
3. Thut, G; Nietzel, A; Brandt, SA; Pascual-Leone, A. Alpha-band electroencephalographic activity over occipital cortex indexes visuospatial attention bias and predicts visual target detection. *J. Neurosci.* **2006**, *26(37)*, 9494-9502; https://doi.org/10.1523/jneurosci.0875-06.2006
4. Klimesch, W; Sauseng, P; Hanslmayr, S. EEG alpha oscillations: the inhibition-timing hypothesis. *Brain. Res. Rev.* **2007**, *53(1)*, 63-88; https://doi.org/10.1016/j.brainresrev.2006.06.003
5. Jensen, O; Mazaheri, A. Shaping functional architecture by oscillatory alpha activity: gating by inhibition. *Front. Hum. Neurosci.* **2010**, *4*, 186; https://dx.doi.org/10.3389%2Ffnhum.2010.00186
6. Gratton, G; Villa, A.E.P; Fabiani, M; Giovanna, C; Palin, E; Bolcioni, G; G. Fiori, M. Functional correlates of a three-component spatial model of the alpha rhythm, Functional correlates of a three-component spatial model of the alpha rhythm. *Brain. Res.* **1992**, *582(1)*, 159-162; https://doi.org/10.1016/0006-8993(92)90332-4
7. Worden, M.S; Foxe, J; Wang, N; Simpson, GV. Anticipatory biasing of visuospatial attention indexed by retinotopically specific-band electroencephalography increases over occipital cortex. *J. Neurosci.* **2000**, *20(6)*,63; https://doi.org/10.1523/jneurosci.20-06-j0002.2000
8. Pfurtscheller, G; Neuper, C. Event-related synchronization of mu rhythm in the EEG over the cortical hand area in man. *Neurosci. Lett.* **1994**, *174(1)*, 93-96; https://doi.org/10.1016/0304-3940(94)90127-9
9. Hanslmayr, S; Aslan, A; Staudigl, T; Klimsch, W; Herrmann, CS; Bäuml, KH. Prestimulus oscillations predict visual perception performance between and within subjects. *Neuroimage.* **2007**, *37(4)*, 1465-1473; https://doi.org/10.1016/j.neuroimage.2007.07.011
10. Van Dijk, H; Schoffelen, J; Oostenveld, R; Jensen, O. Prestimulus oscillatory activity in the alpha band predicts visual discrimination ability. *J. Neurosci.* **2008**, *28(8)*, 1816-1823; https://doi.org/10.1523/JNEUROSCI.1853-07.2008
11. Lerga, J; Saulig, N; Mozetic, V; Lerga, R. Number of EEG signal components estimated using the short-term Rényi entropy. **2016** International Multidisciplinary Conference on Computer and Energy Science (SpliTech). 2016. IEEE. pp.1-6; https://doi.org/10.1109/SpliTech.2016.7555940
12. Lerga, J; Saulig, N; Mozetič, V. Algorithm based on the short-term Rényi entropy and IF estimation for noisy EEG signals analysis. *Comput.Biol.Med*, **2017**. *80*, 1-13; https://doi.org/10.1016/j.compbiomed.2016.11.002

13. Jadav, G.M; Lerga, J; Štajduhar, I. Adaptive filtering and analysis of EEG signals in the time-frequency domain based on the local entropy. *EURASIP. J. Adv. Signal. Process,* **2020**. *2020(1),* 1-18; https://doi.org/10.1186/s13634-020-00667-6
14. Mathewson, K.E; Gratton, G; Fabiani, M; Beck, DM; Ro, T. To see or not to see: prestimulus α phase predicts visual awareness. *J. Neurosci.* **2009**, *29(9),* 2725-2732; https://doi.org/10.1523/jneurosci.3963-08.2009
15. VanRullen, R; Busch, N; Drewes, J; Dubois, J. Ongoing EEG phase as a trial-by-trial predictor of perceptual and attentional variability. *Front. Psychol.* **2011**, *2,* 60; https://dx.doi.org/10.3389%2Ffpsyg.2011.00060
16. Pavlides, C; Greenstein, Y.J; Grudman, M; Winson, J. Long-term potentiation in the dentate gyrus is induced preferentially on the positive phase of θ-rhythm. *Brain. Res.* **1988**, *439(1-2),* 383-387; https://doi.org/10.1016/0006-8993(88)91499-0
17. Hölscher, C; Anwyl, R; Rowan, MJ. Stimulation on the positive phase of hippocampal theta rhythm induces long-term potentiation that can be depotentiated by stimulation on the negative phase in area CA1 in vivo. *J. Neurosci.* **1997**, *17(16),* 6470-6477; https://doi.org/10.1523/jneurosci.17-16-06470.1997
18. Hyman, J.M; Wyble, B.P; Goyal, V; Rossi, CA; Hasselmo, ME. Stimulation in hippocampal region CA1 in behaving rats yields long-term potentiation when delivered to the peak of theta and long-term depression when delivered to the trough. *J. Neurosci.* **2003**, *23(37),* 11725-11731; https://doi.org/10.1523/jneurosci.23-37-11725.2003
19. Chen, L.L, Madhavan, R; Rapoport, BI; Anderson, WS. Real-time brain oscillation detection and phase-locked stimulation using autoregressive spectral estimation and time-series forward prediction. *IEEE. Trans. Biomed. Eng.* **2013**, *60(3),* 753-762; https://doi.org/10.1109/tbme.2011.2109715
20. Zrenner, C; Desideri, D; Belardinelli, P; Ziemann, U. Real-time EEG-defined excitability states determine efficacy of TMS-induced plasticity in human motor cortex. *Brain Stimul.* **2018**, 11(2), 374-389; https://doi.org/10.1016/j.brs.2017.11.016
21. Zrenner, C; Galevska, D; Nieminen, JO; Baur, D; Stefanou, MI; Ziemann, U. The shaky ground truth of real-time phase estimation. *Neuroimage.* **2020**, *214*, 116761; https://doi.org/10.1016/j.neuroimage.2020.116761
22. Roux, SG; Cenier, T; Garcia, S; Litaudon, P; Buonviso, N. A wavelet-based method for local phase extraction from a multi-frequency oscillatory signal. *J. Neurosci. Methods*. **2007**, *160(1),* 135-143; https://doi.org/10.1016/j.jneumeth.2006.09.001
23. McIntosh, JR; Sajda, P. Estimation of phase in EEG rhythms for real-time applications. *J. Neural Eng*. **2020**, *17(3),* 034002; https://doi.org/10.1088/1741-2552/ab8683
24. Ziemann, U; Reis, J; Schwenkreis, P; Rosanova, M; Strafella, A; Badawy, R; Müller-Dahlhaus, F. TMS and drugs revisited 2014. *Clin. Neurophysiol*. **2015**, *126(10),* 1847-1868; https://doi.org/10.1016/j.clinph.2014.08.028
25. Hallett, M; Transcranial magnetic stimulation and the human brain. *Nature*, **2000**. *406(6792),* 147-150; https://doi.org/10.1038/35018000

26. Zrenner, C; Belardinelli, P; Müller-Dahlhaus, F; Ziemann, U. Closed-loop neuroscience and non-invasive brain stimulation: a tale of two loops. *Front. Cell. Neurosci*. **2016**, *10*, 92; https://doi.org/10.3389/fncel.2016.00092
27. Ilmoniemi, RJ; Kičić, D. Methodology for combined TMS and EEG. *Brain Topogr*. **2010**, *22(4)*, 233-248; https://doi.org/10.1007/s10548-009-0123-4
28. Müller-Dahlhaus, F; Vlachos, A. Unraveling the cellular and molecular mechanisms of repetitive magnetic stimulation. *Front. Mol. Neurosci*. **2013,** *6*, 50; https://doi.org/10.3389/fnmol.2013.00050
29. Mutanen, T; Nieminen, JO; Ilmoniemi, RJ. TMS-evoked changes in brain-state dynamics quantified by using EEG data. *Front. Hum. Neurosci*. **2013**, *7*, 155; https://doi.org/10.3389/fnhum.2013.00155
30. Buzsáki, G; Draguhn, A. Neuronal oscillations in cortical networks. *Science*. **2004**, *304(5679)*, 1926-1929; https://doi.org/10.1126/science.1099745
31. Gharabaghi, A; Kraus, D; Leão, MT; Spüler, M; Walter, A; Bogdan, M; Rosenstiel, W; Naros, G; Ziemann, U. Coupling brain-machine interfaces with cortical stimulation for brain-state dependent stimulation: enhancing motor cortex excitability for neurorehabilitation. *Front. Hum. Neurosci.* **2014**, *8*, 122; https://doi.org/10.3389/fnhum.2014.00122
32. Bundy, DT; Wronkiewicz, M; Sharma, M; Moran, DW; Corbetta, M; Leuthardt, EC. Using ipsilateral motor signals in the unaffected cerebral hemisphere as a signal platform for brain–computer interfaces in hemiplegic stroke survivors. *J. Neural Eng.* **2012**, *9(3)*, 036011; https://doi.org/10.1088/1741-2560/9/3/036011
33. Pfurtscheller, G; C, Neuper. Dynamics of sensorimotor oscillations in a motor task, *in Brain-Computer Interfaces*; Springer: Berlin/Heidelberg, Germany, 2009; pp. 47-64; https://doi.org/10.1007/978-3-642-02091-9_3
34. Kraus, D; Naros, G; Bauer, R; Leão, MT; Ziemann, U; Gharabaghi, A. Brain–robot interface driven plasticity: distributed modulation of corticospinal excitability. *Neuroimage*. **2016**, *125*, 522-532; https://doi.org/10.1016/j.neuroimage.2015.09.074
35. Ramos-Murguialday, A; Broetz, D; Rea, M; Läer, L; Yilmaz, O; Brasil, FL; Liberati, G; Curado, MR; Garcia-Cossio, E; Vyziotis, A; Cho, W; Agostini, M; Soares, E; Soekadar, S; Caria, A; Cohen, LG; Birbaumer, N. Brain-machine interface in chronic stroke rehabilitation: a controlled study. *Ann. Neurol*. **2013**, *74(1)*, 100-108; https://doi.org/10.1002/ana.23879
36. Buetefisch C, Heger R, Schicks W, Seitz R, Netz J. Hebbian-type stimulation during robot-assisted training in patients with stroke. *Neurorehabil Neural Repair*. **2011**, *25(7)*, 645-655; https://doi.org/10.1177/1545968311402507
37. Shakeel, A; Tanaka, T; Kitajo, K. Time-Series Prediction of the Oscillatory Phase of EEG Signals Using the Least Mean Square Algorithm-Based AR Model. *Appl. Sci.***2020**, *10(10)*, 3616; https://doi.org/10.3390/app10103616
38. Tseng, SY; Chen, RC; Chong, FC; Kuo, TS. Evaluation of parametric methods in EEG signal analysis. *Med. Eng. Phys*. **1995**, *17(1)*, 71-78; https://doi.org/10.1016/1350-4533(95)90380-T

39. Pardey, J; Roberts, S; Tarassenko, L. A review of parametric modelling techniques for EEG analysis. *Med. Eng. Phys*. **1996**, *18(1)*, 2-11; https://doi.org/10.1016/1350-4533(95)00024-0

40. Gibson, JD; Koo, B; Gray, SD; Filtering of colored noise for speech enhancement and coding. *In IEEE Transactions on Signal Processing*, vol. 39, no. 8, p. 1732-1742, Aug. 1991, https://doi.org/10.1109/78.91144

41. Akaike, H. A new look at the statistical model identification. *IEEE. T. Automat. Contr*. **1974**, *19(6)*, 716-723; https://doi.org/10.1109/TAC.1974.1100705

42. Wu, W R; Chen, P C. Adaptive AR modeling in white Gaussian noise. *IEEE. T. Signal. Process.* **1997**, *45(5)*, 1184-1192; http://dx.doi.org/10.1109/78.575693

43. Widrow, B; Stearns, D.S. *Adaptive Signal Processing*, 1st ed.;Prentice-Hall, Inc:, NJ, United States, **1985**.

44. Poularikas, A.D; Ramadan, Z.M. *Adaptive filtering primer with MATLAB*, 1st ed.; CRC Press: Boca Raton, FL, USA, 2006; pp. 101-135.

45. Boashash, B. Estimating and interpreting the instantaneous frequency of a signal. *Fundam. Proc. IEEE* **1992**, *80*, 520-538; https://doi.org/10.1109/5.135376

46. Schaworonkow, N; Triesch, J; Ziemann, U; Zrenner, C. EEG-triggered TMS reveals stronger brain state-dependent modulation of motor evoked potentials at weaker stimulation intensities. *Brain. Stimul.* **2019**, *12(1)*, 110-118; https://doi.org/10.1016/j.brs.2018.09.009

47. Sase, T; Kitajo, K. The metastable human brain associated with autistic-like traits. *bioRxiv*. **2019**, 855502; https://doi.org/10.1101/855502

48. Kitajo, K; Sase, T. Consistency in macroscopic human brain responses to noisy time-varying visual inputs. *bioRxiv*. **2019**, 645499; https://doi.org/10.1101/645499

49. Suetani, H; Kitajo, K. A manifold learning approach to mapping individuality of human brain oscillations through beta-divergence. *Neurosci. Res*. **2020**, *156*, 188-196; https://doi.org/10.1016/j.neures.2020.02.004

50. Delorme, A; Makeig, S. EEGLAB: an open source toolbox for analysis of single-trial EEG dynamics including independent component analysis. *J. Neurosci. Methods* **2004**, *134(1)*, 9-21; https://doi.org/10.1016/j.jneumeth.2003.10.009

51. Lachaux, J.P; Rodriguez, E; Martinerie, J; Varela, F.J. Measuring phase synchrony in brain signals. *Hum. Brain. Mapp*. **1999**, *8(4)*, 194-208; https://doi.org/10.1002/(SICI)1097-0193(1999)8:4%3C194::AID-HBM4%3E3.0.CO;2-C

52. Zarubin, G; Gundlach, C; Nikulin, V; Bogdan, M. Real-time phase detection for EEG-based tACS closed-loop system. In Proceedings of the 6th International Congress on Neurotechnology, Electronics and Informatics, Seville, Spain, 20–21 September 2018; Volume 1, pp. 13-20; https://doi.org/10.5220/0006927300130020

53. Le Van Quyen, M; Foucher, J; Lachaux, J.P; Rodriguez, E; Lutz, A; Martinerie, J; Varela, F.J. Comparison of Hilbert transform and wavelet methods for the analysis of neuronal synchrony. *J. Neurosci. Methods.* **2001**, *111*, 83-98; https://doi.org/10.1016/S0165-0270(01)00372-7

54. Bajaj, V; Pachori, R.B. Separation of rhythms of EEG signals based on Hilbert-Huang transformation with application to seizure detection. In Proceedings of the International Conference on Hybrid Information Technology, Daejeon, Korea, 23–25 August 2012; Volume 7425, pp. 493-500; https://doi.org/10.1007/978-3-642-32645-5_62

55. Lin, C.F; Zhu, J.D. Hilbert–Huang transformation-based time-frequency analysis methods in biomedical signal applications. *Proc. Inst. Mech. Eng. Part H J. Eng. Med.* **2012**, *226*, 208-216; https://doi.org/10.1177%2F0954411911434246

56. Mansouri, F; Dunlop, K; Giacobbe, P; Downar, J; Zariffa, J. A Fast EEG Forecasting Algorithm for Phase-Locked Transcranial Electrical Stimulation of the Human Brain. *Front. Neurosci.* **2017**, *11*, 401; https://doi.org/10.3389/fnins.2017.00401

57. Fisher, N.I. *Statistical Analysis of Circular Data*; Cambridge University Press: Cambridge, UK, 1995; pp. 69-70; https://doi.org/10.1017/CBO9780511564345

58. Mazaheri, A; Jensen, O. Posterior α activity is not phase-reset by visual stimuli. *Proc. Natl. Acad. Sci. USA* **2006**, *103*, 2948-2952; https://doi.org/10.1073/pnas.0505785103

59. Persson, T. A new way to obtain Watson's U^2. *Scand. Stat. Theory Appl.* **1979**, *6*, 119-122.

60. Ueda, K.I; Nishiura, Y; Kitajo, K. Mathematical mechanism of state-dependent phase resetting properties of alpha rhythm in the human brain. *Neurosci. Res.* **2020**, *156*, 237-244; https://doi.org/10.1016/j.neures.2020.03.007

61. Oh, S.L; Vicnesh, J; Ciaccio, E.J; Yuvaraj, R; Acharya, U.R. Deep convolutional neural network model for automated diagnosis of schizophrenia using EEG signals. *Appli.Sci*. **2019**, 9(14), 2870; https://doi.org/10.3390/app9142870

62. Oh, S.L; Hagiwara, Y; Raghavendra, U; Yuvaraj, R; Arunkumar, N; Murugappan, M; Acharya, U.R. A deep learning approach for Parkinson's disease diagnosis from EEG signals. *Neural. Comput. Appl*. **2018**, *32*, 10927-10933; https://doi.org/10.1007/s00521-018-3689-5

63. Li, F; Li, X; Wang, F; Zhang, D; Xia, Y; He, F. A novel P300 classification algorithm based on a principal component analysis-convolutional neural network. *Appli. Sci.* **2020**, *10*, 1546; https://doi.org/10.3390/app10041546

64. Li, F; He, F; Wang, F; Zhang, D; Xia, Y; Li, X. A Novel Simplified Convolutional Neural Network Classification Algorithm of Motor Imagery EEG Signals Based on Deep Learning. *Appl. Sci.* **2020**, *10*, 1605; https://doi.org/10.3390/app10051605

65. Rosin, B; Slovik, M; Mitelman, R; Rivlin-Etzion, M; Haber, S.N; Israel, Z; Vaadia, E; Bergman, H. Closed-loop deep brain stimulation is superior in ameliorating parkinsonism. *Neuron.* **2011**, *72*, 370-384; https://doi.org/10.1016/j.neuron.2011.08.023

66. Little, S; Brown, P. What brain signals are suitable for feedback control of deep brain stimulation in Parkinson's disease? *Ann. N. Y. Acad. Sci.* **2012**, *1265*, 9-24; https://doi.org/10.1111/j.1749-6632.2012.06650.x

67. Little, S; Pogosyan, A; Neal, S; Zavala, B; Zrinzo, L; Hariz, M; Foltynie, T; Limousin, P; Ashkan, K; Fitzgerald, J; Green, AL; Aziz, TZ; Brown P. Adaptive deep brain stimulation in advanced Parkinson disease. *Ann. Neurol.* **2013**, *74*, 449-457; https://doi.org/10.1002/ana.23951

68. Sun, FT; Morrell, MJ. Closed-loop neurostimulation: the clinical experience. *Neurotherapeutics*. **2014**, *11*, 553-563; https://doi.org/10.1007/s13311-014-0280-3